Atmos. Chem. Phys., 22, 8739–8766, 2022
https://doi.org/10.5194/acp-22-8739-2022

Atmospheric Chemistry and Physics
Open Access
EGU

Polycyclic aromatic hydrocarbons (PAHs) and their alkylated, nitrated and oxygenated derivatives in the atmosphere over the Mediterranean and Middle East seas

Marco Wietzoreck[1], Marios Kyprianou[2], Benjamin A. Musa Bandowe[1], Siddika Celik[3], John N. Crowley[4], Frank Drewnick[3], Philipp Eger[4], Nils Friedrich[4], Minas Iakovides[2], Petr Kukučka[5], Jan Kuta[5], Barbora Nežiková[5], Petra Pokorná[6], Petra Přibylová[5], Roman Prokeš[5,7], Roland Rohloff[4], Ivan Tadic[4], Sebastian Tauer[4], Jake Wilson[1], Hartwig Harder[4], Jos Lelieveld[2,4], Ulrich Pöschl[1], Euripides G. Stephanou[2,8], and Gerhard Lammel[1,5]

[1]Multiphase Chemistry Department, Max Planck Institute for Chemistry, 55128 Mainz, Germany
[2]Climate and Atmosphere Research Centre, Cyprus Institute, 2121 Nicosia, Cyprus
[3]Particle Chemistry Department, Max Planck Institute for Chemistry, 55128 Mainz, Germany
[4]Atmospheric Chemistry Department, Max Planck Institute for Chemistry, 55128 Mainz, Germany
[5]RECETOX, Faculty of Science, Masaryk University, 61137 Brno, Czech Republic
[6]Department of Aerosol Chemistry and Physics, Institute of Chemical Process Fundamentals, The Czech Academy of Sciences, 16502 Prague, Czech Republic
[7]Global Change Research Institute, The Czech Academy of Sciences, 60300 Brno, Czech Republic
[8]Department of Chemistry, University of Crete, 70013 Heraklion, Greece

Correspondence: Gerhard Lammel (g.lammel@mpic.de)

Received: 13 January 2022 – Discussion started: 18 January 2022
Revised: 21 April 2022 – Accepted: 13 May 2022 – Published: 7 July 2022

Abstract. Polycyclic aromatic hydrocarbons (PAHs) and their alkylated (RPAHs), nitrated (NPAHs) and oxygenated (OPAHs) derivatives are air pollutants. Many of these substances are long-lived, can undergo long-range atmospheric transport and adversely affect human health upon exposure. However, the occurrence and fate of these air pollutants have hardly been studied in the marine atmosphere. In this study, we report the atmospheric concentrations over the Mediterranean Sea, the Red Sea, the Arabian Sea, the Gulf of Oman and the Arabian Gulf, determined during the AQABA (Air Quality and Climate Change in the Arabian Basin) project, a comprehensive ship-borne campaign in summer 2017. The average concentrations of $\sum_{26}$PAHs, $\sum_{19}$RPAHs, $\sum_{11}$OPAHs and $\sum_{17}$NPAHs, in the gas and particulate phases, were $2.99 \pm 3.35\,\mathrm{ng\,m^{-3}}$, $0.83 \pm 0.87\,\mathrm{ng\,m^{-3}}$, $0.24 \pm 0.25\,\mathrm{ng\,m^{-3}}$ and $4.34 \pm 7.37\,\mathrm{pg\,m^{-3}}$, respectively. The Arabian Sea region was the cleanest for all substance classes, with concentrations among the lowest ever reported. Over the Mediterranean Sea, we found the highest average burden of $\sum_{26}$PAHs and $\sum_{11}$OPAHs, while the $\sum_{17}$NPAHs were most abundant over the Arabian Gulf (known also as the Persian Gulf). 1,4-Naphthoquinone (1,4-O_2NAP) followed by 9-fluorenone and 9,10-anthraquinone were the most abundant studied OPAHs in most samples. The NPAH composition pattern varied significantly across the regions, with 2-nitronaphthalene (2-NNAP) being the most abundant NPAH. According to source apportionment investigations, the main sources of PAH derivatives in the region were ship exhaust emissions, residual oil combustion and continental pollution. All OPAHs and NPAHs except 2-nitrofluoranthene (2-NFLT), which were frequently detected during the campaign, showed elevated concentrations in fresh shipping emissions. In contrast, 2-NFLT and 2-nitropyrene (2-NPYR) were highly abundant in aged shipping emissions due to secondary formation. Apart from 2-NFLT and 2-NPYR, benz(a)anthracene-7,12-dione and 2-NNAP also had significant photochemical sources. Another finding was that the highest concentrations of PAHs, OPAHs and NPAHs were found in the sub-micrometre fraction of particulate matter (PM_1).

Published by Copernicus Publications on behalf of the European Geosciences Union.

1 Introduction

Air pollution contributes to the global burden of respiratory and cardiovascular diseases (Shiraiwa et al., 2017; Lelieveld et al., 2019). The Red Sea and especially the Arabian Gulf region are prone to major risks by air particulate matter (PM) and gas-phase pollutants due to the hot and arid climate, leading to high dust concentrations and photochemical activity (Lelieveld et al., 2009). In combination with high anthropogenic emissions from highly populated cities, intense marine traffic due to major trade routes (Johansson et al., 2017) and a strong petrochemical industry, air pollution can be significant in these regions (Lelieveld et al., 2015).

One major class of air pollutants is polycyclic aromatic hydrocarbons (PAHs) and their alkylated (RPAHs), nitrated (NPAHs) and oxygenated (OPAHs) derivatives. Several of these substances are classified as carcinogenic or possibly carcinogenic (IARC, 1983, 2012a, b, 2018; OEHHA, 2021). Moreover, many polycyclic aromatic compounds (PACs) show strong mutagenic (Durant et al., 1996; Clergé et al., 2019; Idowu et al., 2019) and ecotoxic effects (El Alawi et al., 2002; Sverdrup et al., 2002a, b; WHO, 2003). Quinones, a major subgroup of OPAHs, have received more attention in recent years due to their potential to contribute to oxidative stress on the cell level (Bolton et al., 2000; Xiong et al., 2017; Lyu et al., 2018). Although some PAH derivatives show even higher toxicity than their parent PAHs (Durant et al., 1996; Collins et al., 1998; WHO, 2003; Turcotte et al., 2011; Lee et al., 2017; IARC, 2018; Clergé et al., 2019; Idowu et al., 2019), their atmospheric concentrations and their cycling and fate are not well studied. Alkylated 3-ring PAHs are more persistent, bioaccumulative and toxic than the parent 3-ring PAHs, which have been identified as substances with persistent, bioaccumulative, and/or toxic properties (PBT) (ECHA, 2021; Wassenaar and Verbruggen, 2021).

PAHs, OPAHs, NPAHs and RPAHs are formed by incomplete combustion of fossil fuels, biomass and waste (Baek et al., 1991; Yunker et al., 2002; Ravindra et al., 2008; Bandowe and Meusel, 2017; Abbas et al., 2018). Apart from these pyrogenic sources, PAHs, especially low-molecular-weight PAHs and RPAHs, and some PAH derivatives can originate from petrogenic sources and spills of petroleum hydrocarbons (Andersson and Achten, 2015; Zhao et al., 2015; Abbas et al., 2018). In addition to these so-called primary emissions, NPAHs and OPAHs can also be formed by secondary formation by reactions of PAHs with atmospheric oxidants (Finlayson-Pitts and Pitts, 1999; Tsapakis and Stephanou, 2007; Walgraeve et al., 2010; Keyte et al., 2013; Bandowe and Meusel, 2017; Abbas et al., 2018). For most PAH derivatives, the contribution from secondary formation is not known. It was shown that 2-nitrofluoranthene (2-NFLT) is formed in gas-phase reactions and was not found in direct emissions, while the opposite was reported for 1-nitropyrene (1-NPYR) (Arey et al., 1986; Atkinson et al., 1990; Bamford and Baker, 2003). Therefore, the ratio 2-NFLT/1-NPYR can be used as an indicator for the relative contributions of secondary formation reactions in the gas-phase compared to primary emitted compounds (Ciccioli et al., 1996; Bamford and Baker, 2003).

The concentration of PAHs in ambient air as well as other environmental compartments has been studied quite extensively in the last decades (Baek et al., 1991; Srogi, 2007; Ravindra et al., 2008), especially for the 16 U.S. EPA-prioritised PAHs (Keith, 2015). However, our knowledge about the distribution of PAH derivatives is still limited (Andersson and Achten, 2015; Lammel, 2015; Bandowe and Meusel, 2017; Jin et al., 2020). There are several studies reporting atmospheric concentrations of OPAHs and NPAHs in the particulate and the gas phase at urban and semi-urban sites (Bamford and Baker, 2003; Albinet et al., 2007, 2008; Garcia et al., 2014; Li et al., 2015; Tomaz et al., 2016; Alves et al., 2017; Kitanovski et al., 2020). Rural/continental background and remote continental sites were investigated in a small number of studies, indicating that several NPAHs and OPAHs are ubiquitous (Ciccioli et al., 1996; Tsapakis and Stephanou, 2007; Albinet et al., 2008; Brorström-Lundén et al., 2010; Scipioni et al., 2012; Tang et al., 2014; Nežiková et al., 2021). Their detection in the Arctic (Drotikova et al., 2021) and the Antarctic (Vincenti et al., 2001; Minero et al., 2010) confirms the long-range transport potential (Keyte et al., 2013). This is supported by global modelling studies of NPAHs (Wilson et al., 2020; Kelly et al., 2021). However, fewer studies have determined the pollutant concentrations in the marine environment, in polluted sea regions or in marine background air. Tsapakis and Stephanou (2007) and Lammel et al. (2017) measured NPAHs and OPAHs at an eastern Mediterranean marine background location, while Zhang et al. (2018) sampled air on Tuoji Island in the Yellow Sea. To the best of our knowledge, there is no study measuring NPAHs and OPAHs over the open ocean. Knowledge about the sources of pollution and the atmospheric fate processes such as gas–particle partitioning, photochemical degradation and deposition in the marine environment is crucial for understanding the distribution and fate of these pollutants, although very little is known (Keyte et al., 2013). In addition, these processes in marine air are crucial for modelling the distribution of these substances, and the concentrations are needed for the validation of modelling results (Wilson et al., 2020; Kelly et al., 2021).

The objective of this study was to determine the concentrations in the gas and particulate phase of the PAHs, RPAHs, NPAHs and OPAHs in the Mediterranean Sea and around the Arabian Peninsula including the Red Sea, Arabian Sea and the Arabian Gulf region. We aimed to study the mass size distributions of PACs in the atmosphere of a hot marine en-

vironment. Furthermore, we provide information about the sources of air pollution in these regions.

2 Methods

2.1 The AQABA ship campaign

The Air Quality and Climate in the Arabian Basin (AQABA) campaign took place in summer 2017 from 25 June until 1 September 2017, sailing on a research vessel (*Kommandor Iona*, IMO registration: 8401999) from Toulon, France, to Kuwait City, and back, with a 2 d stop in Jeddah, Saudi Arabia (first leg), and a 5 d stop in Kuwait. The sampling was performed only during cruise and outside the 12 nmi zones of the countries in the Mediterranean Sea (MS), Suez Canal, Red Sea (RS), Arabian Sea (AS, in the northern Indian Ocean), Gulf of Oman (OG) and the Arabian Gulf (AG, also known as the Persian Gulf). For the evaluation, the Red Sea is split into the northern Red Sea (NRS) and southern Red Sea (SRS). The Suez Canal is included in the northern Red Sea region; the Gulf of Aden is part of the Arabian Sea. The sampling regions and sampling cruises are shown in Fig. S1 in the Supplement.

2.2 Sampling

2.2.1 Air sampling for analysis of PAHs, OPAHs and NPAHs

The air pollutants were sampled separately in gas and particulate phases in polyurethane foams (PUFs; Molintan a.s., Břeclav, Czech Republic) and on quartz microfibre filters (QFFs; QMA type, Whatman, Sheffield, United Kingdom), respectively, by active air sampling on the observation deck (in the front part of the vessel, around 7.7 m a.s.l. and 55 m away from the stack). The aerosol was sampled as PM_{10} (all particles with an aerodynamic equivalent diameter of $< 10\,\mu m$) by a Digitel sampler (DH77, Hegnau, Switzerland). Additionally, PM was collected size-segregated with six size fractions (five stages + backup filter) within PM_{10} ($PM_{<0.49\,\mu m}$ (backup filter), $PM_{0.49–0.95\,\mu m}$, $PM_{0.95–1.5\,\mu m}$, $PM_{1.5–3\,\mu m}$, $PM_{3–7\,\mu m}$ and $PM_{7–10\,\mu m}$) using a high-volume sampler (Baghirra HV 100-P, Prague, Czech Republic) equipped with a cascade impactor inlet (TE-235, Tisch Environmental, Inc., Cleves, USA).

All filters were pre-baked at 300 °C for 12 h, and the PUFs were pre-cleaned (8 h Soxhlet extraction in acetone and 8 h in dichloromethane (DCM); JT Baker, Avantor group, Poland, pesticide residue grade) before wrapping them into two layers of aluminium foil, placing them into zip-lock polyethylene bags and keeping them frozen at −20 °C prior to deployment. After exposure, the samples were wrapped in aluminium foil and kept in polyethylene zip-lock bags at −20 °C during storage. During the whole cruise, 62 air samples (gas- and particulate-phase) and 30 size-resolved PM samples were collected together with three field blanks from each sampler, respectively. Detailed sampling information is provided in Fig. S1 and in Table S1 in the Supplement.

2.2.2 Air sampling for analysis of PAHs and RPAHs

A total of 43 air (gas- and particulate-phase) samples for the determination of PAHs and alkylated PAHs and three field blanks (three PUFs and three QFFs) were collected on the monkey deck of the research vessel (around 4 m higher and 5 m less far away from the stack compared to the samplers for PAHs, OPAHs and NPAHs) during the campaign, using a high-volume air sampler (GMWL-2000H; General Metal Works, Cleves, USA). After sampling, the filters and PUFs were stored similarly as the Digitel high-volume samples. In contrast to the Digitel high-volume sampler, total suspended particles (TSP) instead of PM_{10} were collected. The sampling duration varied from 6 to 24 h (mostly 24 h), and the total volume of each air sample ranged from 318 to 1428 m^3 (mainly around 700 m^3), which was based on the cruise planning but also influenced by limited access to sampling spots on the ship due to either bad weather or other extrinsic conditions on the ship (e.g. power failures or sudden short access restrictions) (Table S1). Pre-combusted QFFs (3 h at 420 °C) and pre-extracted PUF plugs (8.0 × 7.5 cm, Ziemer, Langerwehe, Germany; PUFs were washed with water and soap, rinsed with ultrapure water and boiled in ultrapure water for at least 3 h; excess water was removed, and PUFs were extracted in a Soxhlet device with acetone (Lichrosolv, Merck) for 24 h and with 1 : 1 mixture *n*-hexane / DCM (Unisolv, Merck) for another 24 h) were used for the collection of particulate and gaseous phases, respectively.

2.3 Sample preparation and analysis

2.3.1 PAHs, OPAHs and NPAHs

PUFs and QFFs were extracted using automated Soxhlet extraction (40 min Soxhlet extraction followed by 20 min of solvent rinsing) with DCM (JT Baker, Avantor group, Poland), pesticide residue grade) in a B-811 extraction unit (Büchi, Flawil, Switzerland). Prior to extraction, the samples were spiked with the surrogate standards: deuterated nitro-PAHs (1-nitronaphthalene-d7, 2-nitrofluorene-d9, 9-nitroanthracene-d9, 3-nitrofluoranthene-d9, 1-nitropyrene-d9, 6-nitrochrysene-d11, 6-nitrobenzo[a]pyrene-d11) and deuterated PAHs (naphthalene-d8, phenanthrene-d10, perylene-d12). All analytical standards were purchased from Sigma Aldrich (Darmstadt, Germany) or Chiron (Trondheim, Norway).

The extract was cleaned up using a silica column (with 1 cm i.d. as open tube using 5 g of silica (Merck, Darmstadt, Germany), 0.063–0.200 mm, activated at 150 °C for 12 h, 10 % deactivated with water) and 1 g Na_2SO_4 (Merck, Darmstadt, Germany). The sample was loaded onto the column and the target substances were eluted by 5 mL *n*-hexane (JT

Baker, Avantor group, Poland), pesticide residue grade), followed by 50 mL DCM. The volume of the eluate was then reduced by a stream of nitrogen (purity grade 4.7, SIAD, Czech Republic) in a TurboVap II (Caliper LifeSciences, Mountain View, USA) concentrator unit and transferred into a GC vial, spiked with *p*-terphenyl and PCB 121 (internal injection standards), and the final volume in the vial was adjusted to 200 µL.

Polycyclic aromatic compounds (PACs) in the sample extracts were analysed at the Trace Analytical Laboratory of the research centre RECETOX at the Masaryk University in Brno, Czech Republic, similar to the method described by Nežiková et al. (2021). The target compounds in this analysis were 26 PAHs, 1S-heterocycle, 1 RPAH, 17 NPAHs and 11 OPAHs. All target PAHs, OPAHs and NPAHs including their acronyms are shown in Table 1. The physico-chemical properties of all targeted compounds are shown in Table S2.

The analysis of PAHs was performed by a gas chromatograph (GC; 7890A, Agilent, Santa Clara, USA) equipped with a 60 m × 0.25 mm × 0.25 µm Rxi-5Sil MS column (Restek, Bellefonte, USA) coupled to a mass spectrometer (MS; 7000B triple quadrupole, Agilent, Santa Clara, USA). An amount of 1 µL of sample was injected splitless at a constant temperature of 280 °C with He as carrier gas (purity grade 5.5, SIAD, Czech Republic) at a constant flow rate of 1.5 mL min^{-1}. The GC program was as follows: 80 °C (1 min hold), then heated at a rate of 15 °C min^{-1} to 180 °C, followed by 5 °C min^{-1} to 310 °C (20 min hold). The MS was operated in positive electron ionisation (EI+) mode with selected ion monitoring (SIM). The SIM m/z ratios and the retention times of the targeted PAHs are shown in Table S3a.

NPAHs and OPAHs were analysed by GC atmospheric pressure chemical ionisation tandem mass spectrometry (GC-APCI-MS/MS) on a Waters Xevo TQ-S MS (Waters, Mildford, USA) coupled to a GC (GC 7890, Agilent, Santa Clara, USA). The MS was operated under dry source conditions in multiple reaction monitoring (MRM) mode (N_2 for APCI: purity grade 5.0; Ar as collision gas: purity grade 5.0, SIAD, Czech Republic). The GC was fitted with a 30 m × 0.25 mm × 0.25 µm Rxi-5Sil MS column (Restek, Bellefonte, USA). The injection of 1 µL of the sample was splitless at 270 °C. He was used as carrier gas at a constant flow rate of 1.5 mL min^{-1}. The oven temperature program was as follows: 90 °C (1 min hold), then heated at a rate of 40 °C min^{-1} to 180 °C, followed by 5 °C min^{-1} to 320 °C (6 min hold). The MRM m/z ratios and the retention times of the targeted OPAHs and NPAHs are given in Table S3b. Target compounds were quantified using an internal standard method, with calibration in the range of 1–1000 ng mL^{-1}. Calibration curves were set as linear fit.

2.3.2 RPAHs

For alkylated PAHs, particulate- and gas-phase samples were extracted separately following a procedure described in detail elsewhere (Iakovides et al., 2021) with certain modifications. Briefly, each sample was spiked before the extraction with a known amount of surrogate standard (2–15 ng of phenanthrene-d10, Dr. Ehrenstorfer) and Soxhlet-extracted with 1 : 1 *n*-hexane : DCM (Unisolv, Merck) mixture for 24 h, and each extract was concentrated using a rotary evaporator (Rotavap RV 300, Büchi, Flawil, Switzerland), to 5 mL. Subsequently, 10 % of the extract was used for PAH analysis. The extract for PAH analysis was cleaned up by liquid–liquid partitioning with 5 % deactivated-DMF (N,N dimethylformamide containing 5 % water) / *n*-hexane for the isolation of polyaromatic from the aliphatic compounds (N,N DMF, Suprasolv, Merck). The aromatic compound fraction was subsequently loaded into a micro-column of non-activated granular silica gel (0.015–0.040 mm, Merck) and anhydrous sodium sulfate (ACS reagent, Sigma-Aldrich), in order to remove any water/DMF traces (Iakovides et al., 2019). Subsequently, the eluents were reduced to approximately 0.3 mL by rotary evaporation evaporation (using a rotary evaporation system (Rotavap RV 300, Büchi), vacuum electronically controlled, no heating of the water bath), transferred with isooctane (Suprasolv, Merck) to 1.1 mL GC vials and further evaporated almost to dryness under a gentle stream of nitrogen (purity grade 5.0) at −10 °C to minimise evaporation losses. Prior to GC/MS analysis, a known amount of internal injection standard mixture (4–20 ng of anthracene-d_{10} in isooctane) was added in each GC vial to assess the recovery of the surrogate standard phenanthrene-d10 (Dr. Ehrenstorfer) in the collected samples. The sample extracts were analysed at the Cyprus Institute (Cyprus). The target compounds in this analysis were phenanthrene (PHE) and 18 RPAHs, which are shown in Table 1.

The analysis was carried out on a GC (7890N GC, Agilent, Santa Clara, USA) equipped with a deactivated fused silica guard column (5 m, Agilent, Santa Clara, USA) followed by a 30 m × 0.25 mm × 0.25 µm fused silica column (DB-5MS, J&W, Santa Clara, USA). The GC was coupled to a mass selective detector (5977B Inert MSD, Agilent, Santa Clara, USA) operating in EI mode. Either 1 or 2 µL of the final extract was injected into the column using a cool on-column inlet (80 °C constant temperature) with a column flow rate of 1.0 mL min^{-1}. The GC oven program was modified to 80 °C initial temperature, held for 1 min, heated at a rate of 21 °C min^{-1} to 150 °C, 5 °C min^{-1} to 300 °C and finally held for 20 min (54 min total run time). The transfer line was kept at 300 °C, while the MS quadrupole and ion source temperature were held at 150 and 230 °C, respectively. Molecular ions used for the identification are shown in Table S3c.

Table 1. Target compounds and their acronyms. CAS numbers and physicochemical properties are shown in Table S2.

Compound	Acronym	Compound	Acronym
Polycyclic aromatic hydrocarbons:	**PAHs**	1,3-/2,10-/3,9-/3,10- Dimethylphenanthrene	1,3-/2,10-/3,9-/1,10-M_2PHE
Acenaphthylene	ACY	1,7-Dimethylphenanthrene	1,7-M_2PHE
Acenaphthene	ACE	2,3-Dimethylphenanthrene	2,3-M_2PHE
Fluorene	FLN	1,9-/4,9- Dimethylphenanthrene	1,9-/4,9-M_2PHE
Phenanthrene	PHE	1,8-Dimethylphenanthrene	1,8-M_2PHE
Anthracene	ANT	Retene (1-methyl-7-isopropylphenanthrene)	RET
Fluoranthene	FLT	**Oxygenated PAHs:**	**OPAHs**
Pyrene	PYR	1,4-Naphthoquinone	1,4-O_2NAP
Benzo(b)fluorene	BBN	Naphthalene-1-aldehyde	1-(CHO)NAP
Benzo(ghi)fluoranthene	BGF	9-Fluorenone	9-OFLN
Cyclopenta(cd)pyrene	CCP	9,10-Anthraquinone	9,10-O_2ANT
Benzo(a)anthracene	BAA	1,4-Anthraquinone	1,4-O_2ANT
Triphenylene	TPH	9,10-Phenanthrenequinone	9,10-O_2PHE
Chrysene	CHR	11H-Benzo(a)fluoren-11-one	11-OBaFLN
Benzo(b)fluoranthene	BBF	11H-Benzo(b)fluoren-11-one	11-OBbFLN
Benzo(j)fluoranthene	BJF	Benzanthrone (7H-benz(de)anthracene-7-one)	BAN
Benzo(k)fluoranthene	BKF	Benz(a)anthracene-7,12-dione	7,12-O_2BAA
Benzo(e)pyrene	BEP	5,12-Naphthacenequinone	5,12-O_2NAC
Benzo(a)pyrene (benzo(def)chrysene)	BAP	**Nitrated PAHs:**	**NPAHs**
Perylene	PER	1-Nitronaphthalene	1-NNAP
Indeno(123-cd)pyrene	INP	2-Nitronaphthalene	2-NNAP
Dibenz(ah)anthracene	DBA	3-Nitroacenaphthene	3-NACE
Dibenz(ac)anthracene	DCA	5-Nitroacenaphthene	5-NACE
Benzo(ghi)perylene	BPE	2-Nitrofluorene	2-NFLN
Anthanthrene	ATT	9-Nitroanthracene	9-NANT
Coronene	COR	9-Nitrophenanthrene	9-NPHE
Benzonaphthothiophene	BNT	3-Nitrophenanthrene	3-NPHE
Alkylated PAHs:	**RPAHs**	2-Nitrofluoranthene	2-NFLT
1-Methylphenanthrene	1-MPHE	1-Nitropyrene	1-NPYR
2-Methylphenanthrene	2-MPHE	2-Nitropyrene	2-NPYR
3-Methylphenanthrene	3-MPHE	7-Nitrobenzo(a)anthracene	7-NBAA
4-Methylphenanthrene	4-MPHE	6-Nitrochrysene	6-NCHR
3,6-Dimethylphenanthrene	3,6-M_2PHE	1,3-Dinitropyrene	1,3-N_2PYR
2,6-Dimethylphenanthrene	2,6-M_2PHE	1,6-Dinitropyrene	1,6-N_2PYR
2,7-Dimethylphenanthrene	2,7-M_2PHE	1,8-Dinitropyrene	1,8-N_2PYR
1,6-/2,9- Dimethylphenanthrene	1,6-/2,9-M_2PHE	6-Nitrobenzo(a)pyrene	6-NBAP

2.4 Supporting parameters

Further description of analytical methods and other supporting parameters such as meteorological data, PM_{10} mass and concentrations of transition metals, elemental carbon (EC) and organic carbon (OC) can be found in the Supplement. The methods and the resulting data of other additional supporting parameters during the AQABA campaign used in this paper are reported in the following studies: (a) the ship exhaust filter, black carbon (BC; using a multiwavelength aethalometer, AE33, Magee Scientific, Berkeley, USA) and surface PAH concentrations using a photoelectric PAH sensor (EcoChem PAS2000, Ansyco, Karlsruhe, Germany) as well as bypassing ships, potentially influencing the sampled air, in Celik et al. (2020); (b) O_3, nitrogen oxides (NO_x, i.e. $NO + NO_2$) and OH radicals in Tadic et al. (2020); (c) O_3, NO_2 and SO_2 in Eger et al. (2019); and (d) NO_x and NO_y (i.e. NO_x + organic and inorganic oxides of nitrogen) in Friedrich et al. (2021). Measurements of OH radicals were done using the HydrOxyl Radical measurement Unit based on fluorescence Spectroscopy (HORUS) instrument (Martinez et al., 2010; Hens et al., 2014), with the inlet pre-injector (IPI) modification (Novelli et al., 2014). The measurement of the actinic flux was done by a spectral radiometer as described in Meusel et al. (2016). The measurement of polychlorinated biphenyls (PCBs), hexachlorocyclohexanes (HCHs), dichlorodiphenyltrichloroethane and isomers (DDX), and other organochlorine pesticides (drins) from the same samples as used for the measurement of PAHs, OPAHs and NPAHs was done as described in Lammel et al. (2016).

2.5 Aerosol source apportionment

Positive matrix factorisation (EPA PMF 5.0) was applied to the PM_{10} chemical composition. PMF was run using two different groups of parameters as input variables using the concentrations of OC, EC and metals in both PMF groups and the sum of PCBs, HCHs, DDX, drins, PAHs, NPAHs and OPAHs only in group 1 and selected individual PAHs, OPAHs and NPAHs in group 2 to obtain source profiles and their contributions to PM_{10} mass. In addition, we added Na^+ as input parameter. However, it has to be considered that the data coverage was only about 65 % of the sampling time. The PMF input species were selected based on following criteria: trace species with focus on PACs, data above the limit of quantification (LOQ), signal-to-noise ratio (S/N) and last, but not least, the matrix dimension limitation. All Digitel high-volume samples were considered in the PMF runs including those with contamination from the ship's stack. The data matrix was prepared in compliance with the procedure described by Polissar et al. (1998); (i) data below the LOQ were replaced with the value LOQ/2, and $(5/6) \cdot$ LOQ was used as the corresponding uncertainty value, and (ii) for missing data geometric mean of species value and a multiple of 3 for the uncertainty value was utilised. The final matrices had 62 samples with 26 and 29 species in group 1 and 2, respectively including total variable. To estimate the optimal number of sources, the PMF model was run several times with different model settings and 3 to 7 factors tested. The Q values (Q_{true}, Q_{robust} and $Q_{\text{expected/theoretical}}$), the resulting source profiles, and the scaled residuals were examined. The optimum number of factors was chosen based on an adequate fit of the model to the data, as shown by the scaled residual histograms and physically interpretable results. The most stable solutions were found for 6 factors by extra modelling uncertainties of 24 % and 18 % for group 1 and group 2, respectively and by exclusion of 3 % and 2 % of the samples by iteration. The correlation between observed and modelled species was $r^2 = 0.75$ and $r^2 = 0.74$ for group 1 and group 2, respectively. All runs converged, the scale residuals were normally distributed and no swaps were observed with the displacement error analysis, indicating that there was limited rotational ambiguity (Table S9).

In addition, principal component analysis (PCA) was performed. Similar to the PMF, all samples were included in the analysis. The concentrations of the selected substances (based on detection frequency and importance for interpretation; i.e. 2-NNAP; 2-NFLT; 1-NPYR; 2-NPYR; 7-NBAA; 1-(CHO)NAP; 9-OFLN; 9,10-O_2ANT; 11-OBaFLN; 11-OBbFLN; BAN; 7,12-O_2BAA; 5,12-O_2NAC; 3-ring PAHs; 4-ring PAHs and 5-7-ring PAHs) were normalised by the total concentration of the NPAHs, OPAHs and PAHs, respectively. In addition, the concentration of EC, OC and the diagnostic ratios BAP / (BAP + BEP), low-molecular-weight PAHs / high-molecular-weight PAHs, 2-NFLT / 1-NPYR; 2-NFLT / 2-NPYR as well as the ratios of the PAH derivatives and their respective parent PAHs were included in the PCA.

2.6 Air mass origin

Residence time distributions of air mass histories, 10 d backward in time, were studied using the FLEXPART Lagrangian particle dispersion model (FLEXPART version 10.4; Pisso et al., 2019), with ECMWF meteorological data (0.5° × 0.5°, 3-hourly; Seibert and Frank, 2004; Stohl et al., 2005). The output is a measure of the time the computational particles (fictive air parcels) resided in grid cells. Per 24 h sampling time, 100 000 particles were released at a height of 100 m a.s.l.

2.7 Quality control

More information about the analytical quality assurance such as the filtering of the samples against contamination by the own ship exhaust, the detailed quality control of the analysis of the PAH derivatives (recoveries of the surrogate standards, blank correction, detection frequencies, limits of quantification (LOQs)) and a summary of PMF diagnostics is given in the Supplement (Sect. S1.5). In short, the recovery of the surrogate standards of the high-volume samples ranged 41 %–119 %. The reported concentrations are blank-corrected using the average of three field blanks but not recovery-corrected. The instrumental limits of quantification (iLOQs) of the PAHs, OPAHs and NPAHs ranged 0.10–53, 0.11–1.96 (ignoring 9,10-phenanthrenequinone) and 0.02–8.33 ng per sample, respectively. For the evaluation, the maximum of the iLOQ and the LOQ of field blank samples (fbLOQs) were used. The fbLOQs of the PAHs, OPAHs and NPAHs ranged 0.12–54.64, < iLOQ–72.76 and < iLOQ–2.67 ng per sample, respectively. The method uncertainty for all target compounds ranged between 4 % and 28 %.

The separation of the isomers 2-NFLT and 3-NFLT is incomplete using the 5MS GC column ((5 %-phenyl-)methylpolysiloxane GC stationary phase). In this study, the separation of the two isomers was inadequate to quantify both isomers separately but sufficient to qualitatively report that 3-NFLT was either not detected or only detected as a small shoulder of the 2-NFLT peak, which was not integrated for the peak area of 2-NFLT.

3 Results and discussion

3.1 Occurrence of PAHs and PAH derivatives

The average total (sum of gas- and particulate-phase) concentrations of the pollutants in the different sea regions are shown in Fig. 1. The average total concentrations (range in brackets) of the sum of one pollutant class from all high-volume air samples of the $\sum_{26}$PAHs, $\sum_{19}$RPAHs, $\sum_{11}$OPAHs and $\sum_{17}$NPAHs were 2.99 ± 3.35 (0.15–17.34) ng m^{-3}, 0.85 ± 0.87 (0.19–3.41) ng m^{-3}, 0.24 ± 0.25

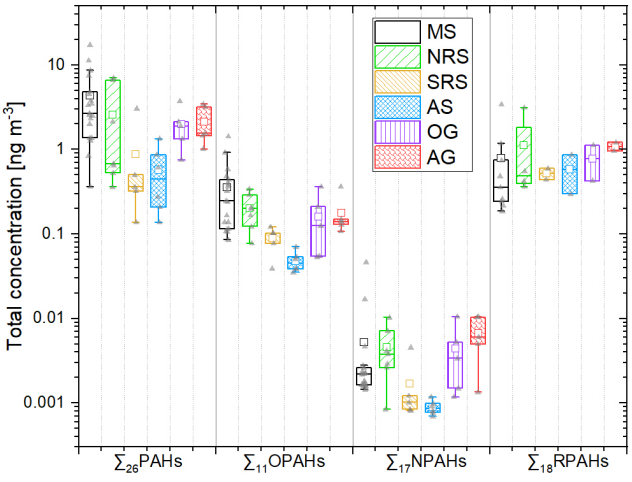

Figure 1. Total concentration (gas + particulate phase) of PAC groups across sea regions. MS: Mediterranean Sea; NRS: northern Red Sea; SRS: southern Red Sea; AS: Arabian Sea; OG: Gulf of Oman; and AG: Arabian Gulf. Empty square: mean value. Grey triangles: measurement points (difficult to see within the boxes). Box with additional borders: interquartile range (IQR) bound by the 75th and 25th percentile and range of 1.5 IQR. Horizontal line: median.

(0.04–1.42) ng m^{-3} and 4.34 ± 7.37 (0.69–46.50) pg m^{-3}, respectively. The $\sum_{26}$PAHs include the S-heterocycle BNT. The concentration range of the $\sum_{19}$RPAHs does not include RET since it cannot be allocated to the individual samples since RET was sampled with another sampler than the other RPAHs. Particulate-phase PAHs, OPAHs and NPAHs were sampled as PM_{10}, while RPAHs were collected as TSP. The difference of PAC concentrations in TSP compared to PM_{10} is expected to be non-significant as reported by Menichini and Monfredini (1995) and Ringuet et al. (2012b) for PAHs and PAH derivatives due to low concentrations of PACs in coarse-mode particles. All the data are filtered for contamination with the stack of our research vessel (details given in Sect. S1.5.1). The detection frequencies of the compounds in the high-volume samples are shown in Fig. S1. All targeted PAHs, RPAHs and OPAHs were detected at least in one sample. From the 17 targeted NPAHs, 7 were detected in at least one high-volume sample. All total concentrations of the individual compounds and individual samples can be found in the Supplement, Tables S10–S14. Individual phases' concentrations are presented and discussed in a separate communication.

The spatial distribution of the concentrations of the different substance classes in both legs is shown in Fig. 2. The plot only shows the average concentration of each sampling stretch, which could also be impacted by individual local plumes at distinct times and locations. Furthermore, it needs to be considered that the method uncertainty at very low concentrations can be relatively high (up to 28 %, see Sect. S1.5.2.2), similar to some of the spatial gradients indicated in Fig. 2. As visible in Figs. 1 and 2, the cleanest region, with the lowest concentration of all substance classes, was the Arabian Sea in the Indian Ocean. The average air concentrations over the Arabian Sea were 0.59 ng m^{-3}, 0.59 ng m^{-3}, 47.8 pg m^{-3} and 0.89 pg m^{-3} for the $\sum_{26}$PAHs, $\sum_{19}$RPAHs, $\sum_{11}$OPAHs and $\sum_{17}$NPAHs, respectively. The air masses originated from the Indian Ocean and from parts of Somalia with no significant sources of PAHs or PAH derivatives (Fig. S3d). Similarly, findings from the same campaign for other air pollutants showed the lowest concentration over the Arabian Sea (Bourtsoukidis et al., 2019; Eger et al., 2019; Pfannerstill et al., 2019; Tadic et al., 2020; Wang et al., 2020). As shown in Fig. 2a, c and e, several samples in the Arabian Sea are missing in the first leg due to rejection as being possibly contaminated by the stack of our research vessel *Kommandor Iona* (detailed overview of rejected samples and method description in Table S4 and Sect. S1.5.1, respectively). The Mediterranean Sea showed the highest average concentration of the $\sum_{26}$PAHs and $\sum_{11}$OPAHs, i.e. 4.40 and 0.37 ng m^{-3}, respectively. As illustrated in Fig. 2, the pollutant concentration over the Mediterranean Sea during the first leg differed from that of the second leg. The concentration of the $\sum_{26}$PAHs during the first leg (2.20 ng m^{-3}) was significantly lower ($p < 0.05$, Student's t test) than during the second leg (5.18 ng m^{-3}). The difference was also significant ($p < 0.05$, Student's t test) for the $\sum_{11}$OPAHs. The air mass histories (Figs. S2 and S3a) reveal that the difference is related to the different origin of the air masses. During the first leg, the sampled air predominantly originated from northern Africa and the western Mediterranean Sea, while during the second leg, the prevailing air masses came from north, transporting polluted air from large parts of Europe, including coastal areas and islands, as also reported by Tadic et al. (2020). The northerly wind is a typical large-scale circulation pattern in summer over the Mediterranean Sea (Lelieveld et al., 2002). The highest concentrations of the PAH derivatives throughout the entire cruise were found in sample D58 in the Mediterranean Sea close to Sicily (coordinates in Table S1). The concentrations of $\sum_{11}$OPAHs and $\sum_{17}$NPAHs were 1.42 ng m^{-3} and 46.5 pg m^{-3}, respectively. Sample D54, sampled 400 km southeast of Sicily (coordinates in Table S1), showed the highest concentration of the $\sum_{26}$PAHs, especially of the low-molecular-weight PAHs (3-ring PAHs). These samples will be evaluated in more detail in Sect. 3.3.4.

The concentration of the $\sum_{17}$NPAHs was similar during both legs in the Mediterranean Sea. On the one hand, 2-NFLT and 2-NPYR were more abundant during the first leg, possibly due to higher secondary formation in aged air (Arey et al., 1986; Atkinson and Arey, 1994). On the other hand, the primarily emitted 1-NPYR (Atkinson and Arey, 1994; Zielinska et al., 2004; Keyte et al., 2016; Srivastava et al., 2018) as well as 2-NNAP (having primary and secondary sources, Atkinson and Arey, 1994; Zhuo et al., 2017) had a higher concentration during the second leg. In contrast to

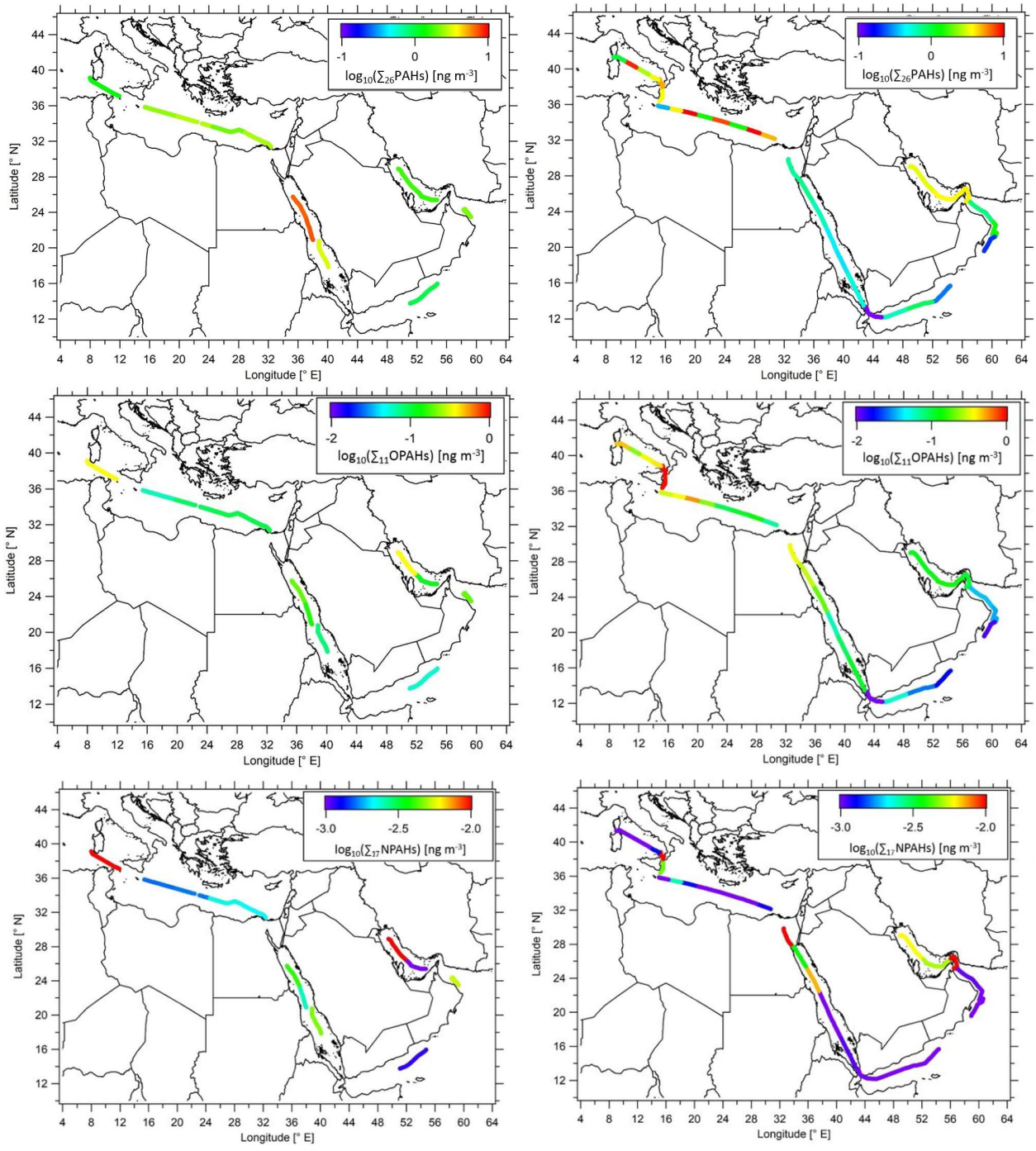

Figure 2. Total concentration (logarithmic scale) of $\sum_{26}$PAHs in **(a)** and **(b)**, $\sum_{11}$OPAHs in **(c)** and **(d)**, and $\sum_{17}$NPAHs in **(e)** and **(f)** during the first leg in **(a)**, **(c)** and **(e)** and the second leg in **(b)**, **(d)** and **(f)**. Spatial resolution of data limited to sampling stretches (see Fig. S1).

the PAHs and OPAHs, the concentration of the $\sum_{19}$RPAHs in the air over the Mediterranean Sea was higher (not significant, $p = 0.14$, Student's t test) and not lower during the first leg compared to the second leg. The different result for the RPAHs can firstly be explained by the different sampling intervals of the air sampler for the RPAHs (see Table S1). The RPAHs were not collected at the end of the campaign close to Sicily and Sardinia, where a high burden of PACs was measured. Second, north of Egypt in the Mediterranean Sea, close to the Suez Canal during the first leg, high con-

centrations of the MPHEs and M_2PHEs were found, possibly due to intense marine traffic concentration or even queueing before entering into the Suez Canal.

The average concentration of the $\sum_{17}$NPAHs over the Mediterranean Sea was 5.23 pg m^{-3}, which was comparable but slightly higher than over the northern Red Sea (4.52 pg m^{-3}) and the Gulf of Oman (4.37 pg m^{-3}) but slightly lower than over the Arabian Gulf (6.65 pg m^{-3}). The concentration of the $\sum_{19}$RPAHs over the Mediterranean Sea (0.81 ng m^{-3}) was similar to the Gulf of Oman (0.83 ng m^{-3}) and comparable but lower than over the Arabian Gulf (1.12 ng m^{-3}), too. Similar to the NPAHs and RPAHs, most other air pollutants (e.g. non-methane hydrocarbons, carbonyl compounds, NO_x, NO_z, O_3, SO_2) measured during the AQABA campaign showed the highest concentration in the Arabian Gulf (Bourtsoukidis et al., 2019; Eger et al., 2019; Pfannerstill et al., 2019; Tadic et al., 2020; Wang et al., 2020; Friedrich et al., 2021).

The concentration of the $\sum_{17}$NPAHs over the southern Red Sea was 1.68 pg m^{-3}. Similar as for the $\sum_{17}$NPAHs, the southern Red Sea was the region with the second lowest concentrations of the $\sum_{26}$PAHs and the $\sum_{11}$OPAHs (0.93 ng m^{-3} and 88.3 pg m^{-3}, respectively). The pollutant burden was low since the air was predominantly coming from eastern Africa, mainly from Sudan, Eritrea, and western and southern parts of Egypt (Fig. S3c), areas with low population and industrial emitter densities. Air over the northern Red Sea, including the Suez Canal, is more polluted, owing to the dense shipping traffic in the canal (Bourtsoukidis et al., 2019), the vicinity of the megacity Cairo and the densely populated and urbanised Nile Delta. The total concentration of the $\sum_{19}$RPAHs over the northern Red Sea was 0.93 ng m^{-3}. The highest concentration was measured in air close to Jeddah, which was more polluted than the other samples by almost 1 order of magnitude.

As shown in Fig. 1, the Gulf of Oman and the Arabian Gulf were similarly polluted as the northern Red Sea. The concentrations of the $\sum_{26}$PAHs and the $\sum_{11}$OPAHs were higher (but not significantly according to Student's t test) in the Arabian Gulf (2.8 ng m^{-3} and 181 pg m^{-3}, respectively) compared to the Gulf of Oman (2.0 ng m^{-3} and 161 pg m^{-3}, respectively). The air masses sampled in the Gulf of Oman were mainly transported from Oman, United Arab Emirates, Iran and the Arabian Sea (Fig. S3e). The predominant wind direction in the Arabian Gulf during the first leg was northwest, transporting air from Qatar, Bahrain, Kuwait and Iraq (Fig. S3f, 28–30 July 2017), while during the second leg, the wind changed to northeast, increasing the contribution of air advected from Iran (Fig. S3f, 4–6 August 2017). A significantly higher ($p < 0.05$, Student's t test) concentration of the $\sum_{26}$PAHs prevailed during advection from northeast (second leg, 3.53 ng m^{-3}) than from northwest (first leg, 1.69 ng m^{-3}).

Comparison to literature

The concentrations of the PAH derivatives in a few samples in the remote sea regions were among the lowest ever reported in air (Walgraeve et al., 2010; Bandowe and Meusel, 2017; Abbas et al., 2018), while other samples reached concentration levels previously found at suburban sites. The samples from near Sicily and Sardinia in the Mediterranean Sea, near the Suez Canal and over the Gulfs showed a total concentration of 0.1–1.4 ng m^{-3} and 1.2–47 pg m^{-3} for the $\sum_{11}$OPAHs and $\sum_{17}$NPAHs, respectively. The concentrations of the individual substances are similar to air samples from a rural and an urban site in Chile (Scipioni et al., 2012), rural sites in France (Albinet et al., 2007, 2008), a suburban site in the USA (Bamford and Baker, 2003) and a background site in the Czech Republic (Nežiková et al., 2021).

NPAHs and OPAHs have rarely been examined in the marine environment. A study by Lammel et al. (2017) investigated the 3–4-ring NPAHs in the eastern Mediterranean under the influence of long-range transport from central and eastern Europe in summer 2012. The concentration of the $\sum_{11}$3–4-ring NPAHs (23.7 pg m^{-3}) was 1 order of magnitude higher than the concentration of the sum of the same NPAHs in the Mediterranean Sea in our study (2.8 pg m^{-3}). The concentration of the samples with the lowest urban influence, found by Lammel and colleagues, was closer to our observed concentrations. In contrast to the NPAHs, the concentration of the $\sum_{6}$4-ring PAHs was in the same order of magnitude. Lammel and colleagues found 426 pg m^{-3} as average of all samples and 284 pg m^{-3} as average of the samples with the lowest urban influence, while we determined a concentration of 366 pg m^{-3} for the sum of the same PAHs. From the same study, Lammel et al. measured 1-NPYR, 2-NFLT and 2-NPYR in marine background air as 0.21, 1.68 and 0.92 pg m^{-3}, whereas respective concentrations were 0.4, 0.9 and 0.1 pg m^{-3} in air over the whole transect of the Mediterranean Sea of our campaign. The lower levels of secondarily formed 2-NFLT and 2-NPYR can be explained by significant long-range transport from NO_x-poor areas, notably northern Africa during the first leg. One decade earlier, in the eastern Mediterranean Sea in summer 2001, Tsapakis and Stephanou (2007) report values that are approximately 1 order of magnitude higher, i.e. 29 and 21 pg m^{-3} for 2-NFLT and 2-NPYR, respectively. Furthermore, they determined 9,10-O_2ANT and 9-OFLN (34.2 and 46.3 pg m^{-3}, respectively), which were in the same range as our measurements in the Mediterranean Sea with 95.4 and 36.2 pg m^{-3}, respectively.

The concentrations of NPAHs (40, 90 and 60 pg m^{-3} for 1-NPYR, 2-NFLT and 2-NPYR, respectively) in source regions of the Mediterranean such as Athens (Marino et al., 2000) were approximately 3 orders of magnitude higher than those in our study over the Mediterranean Sea. This urban to marine background gradient is a lot smaller for the OPAHs compared to the NPAHs. In summer 2013, at a suburban site

in Athens, Alves et al. (2017) found an air concentration of 9, 28 and 242 pg m^{-3} for 9,10-O_2ANT, 9-OFLN and BAN, respectively. This is 1 order of magnitude lower for 9,10-O_2ANT, the same magnitude for 9-OFLN and 1 order of magnitude higher for BAN compared to our results in the Mediterranean Sea. This suggests longer lifetimes or higher formation rates of OPAHs than NPAHs.

Harrison et al. (2016) measured PAHs and their derivatives at three sites along the east coast of the Red Sea, in a plume of a major point source (petrochemical complex). 9,10-O_2ANT had a concentration between 3.15 and 4.02 ng m^{-3}, which is 2 orders of magnitude higher than in the particulate phase of samples over the northern Red Sea in our study. The concentration of 5,12-O_2NAC was between 1 and 2 orders of magnitude higher, while the difference was smaller for 7,12-O_2BAA. The difference of the individual NPAHs concentrations between the measurements at the coast from Harrison et al. (2016) and our measurements offshore is even more pronounced. The concentrations of 2-NNAP, 2-NFLT, 1-NPYR, 2-NPYR and 7-NBAA were over 3 orders of magnitude higher in the plume measured by Harrison et al. (2016) In contrast, the PAH concentration was almost similar (for low-molecular-weight PAHs) or only 1 order of magnitude higher (for high-molecular-weight PAHs, i.e. 5–7-ring PAHs) onshore. This, again, points to short atmospheric lifetimes of NPAHs. The OH reaction rate coefficients of PAHs and NPAHs are similar (Table S2, US EPA, 2019), but NPAHs are more prone to photolysis (Fan et al., 1996; Keyte et al., 2013; Wilson et al., 2020). This is furthermore supported by findings that the NPAH / PAH ratios in mid-latitudes are higher in winter than in summer, obviously since the photochemical sink of NPAHs in summer overcompensates for the higher formation potential as a source of NPAHs (Nežiková et al., 2021). Nassar et al. (2011) measured PAHs and two NPAHs in the area of Greater Cairo. The concentration of 1-NPYR in the study was around 1 order of magnitude higher than that in the air measured on the ship over the Suez Canal. In contrast, the concentration of the low-molecular-weight PAHs was in the same range, while the concentrations of high-molecular-weight PAHs offshore were 1 or more orders of magnitude lower.

Few studies report MPHE and M_2PHE in the coastal marine atmosphere, the open sea, background and urban sites. Tsapakis and Stephanou (2005) analysed atmospheric samples collected offshore over the eastern Mediterranean Sea and at a background station in northeastern Crete (Greece) and reported total (gas- and particulate-phase) concentrations for $\sum$MPHE of 13.6 ng m^{-3} and for $\sum M_2$PHE of 6.5 ng m^{-3}, respectively. Mandalakis et al. (2002) reported gas- and particulate-phase concentrations of 6.07 and 3.17 ng m^{-3} for $\sum$MPHE and $\sum M_2$PHE, respectively, in the Saronikos Gulf, which is impacted by busy marine traffic and the shipyard industry along the coast (Valavanidis et al., 2008). In the same study, corresponding concentrations of 6.95 ng m^{-3} for $\sum$MPHE and of 4.17 ng m^{-3} for $\sum M_2$PHE were reported for the urban atmosphere of Athens and respectively 0.52 and 0.34 ng m^{-3} for the background urban agglomeration. The concentrations in our study were comparable to the background concentrations, i.e. 0.51 and 0.33 ng m^{-3} for $\sum$MPHE and $\sum M_2$PHE, respectively.

The results of the $\sum$MPHE in the gas phase (0.47 ng m^{-3}) in our study are also comparable to concentrations over the southeastern Mediterranean Sea and the Aegean Sea measured by Castro-Jiménez et al. (2012), i.e. 0.58 and 0.61 ng m^{-3}, respectively, but lower than over the western Mediterranean Sea, the Ionian Sea and the Black Sea. On an Atlantic Ocean transect from the Netherlands to South Africa, concentrations of 1-MPHE as low as 0.022 ng m^{-3} were reported, compared to 0.45 ng m^{-3} for samples taken closer to Europe and western Africa (Jaward et al., 2004). In our study 1-MPHE ranged between 0.026 and 0.49 ng m^{-3}.

3.2 Composition patterns

3.2.1 PAHs

The substance patterns of PAHs in the six different sea regions are shown in Fig. 3a. PHE was by far the most abundant PAH in all regions (average contribution of 49 %), followed by FLN, ACE, FLT and PYR, with average contributions of 24 %, 10 %, 6 % and 5 %, respectively. The predominance of 3-ring PAHs was also found in earlier studies of the marine atmosphere (Ding et al., 2007; van Drooge et al., 2010; Lohmann et al., 2013; Kim and Chae, 2016; González-Gaya et al., 2019). It can be noted that the PAH composition patterns were similar in all regions. However, the patterns of the Mediterranean Sea and the southern Red Sea differed from the other regions. The contribution of PHE in the southern Red Sea was higher than the average, while it was lower than the average in the Mediterranean Sea. The opposite could be observed for FLN. The different pattern in the Mediterranean Sea was mainly caused by the samples from the second leg with high influence of aerosols from Europe.

3.2.2 RPAHs

The distribution pattern of RPAHs among the campaign regions is presented in Fig. 3b. The RPAHs did not show significant regional differences in the composition pattern. 2-MPHE, 1-MPHE and 3-MPHE were the most abundant alkylated PAH species throughout the campaign, making up 22 %, 16 % and 12 % of the total RPAHs measured. Among the M_2PHEs, 1,6- and 2,9-M_2PHE were the most abundant compounds.

3.2.3 OPAHs

As shown in Fig. 3c, the regional differences between the OPAH composition patterns are more pronounced than the regional average PAH and RPAH patterns. 1,4-O_2NAP, 9,10-O_2ANT and 9-OFLN were the most abundant OPAHs, with

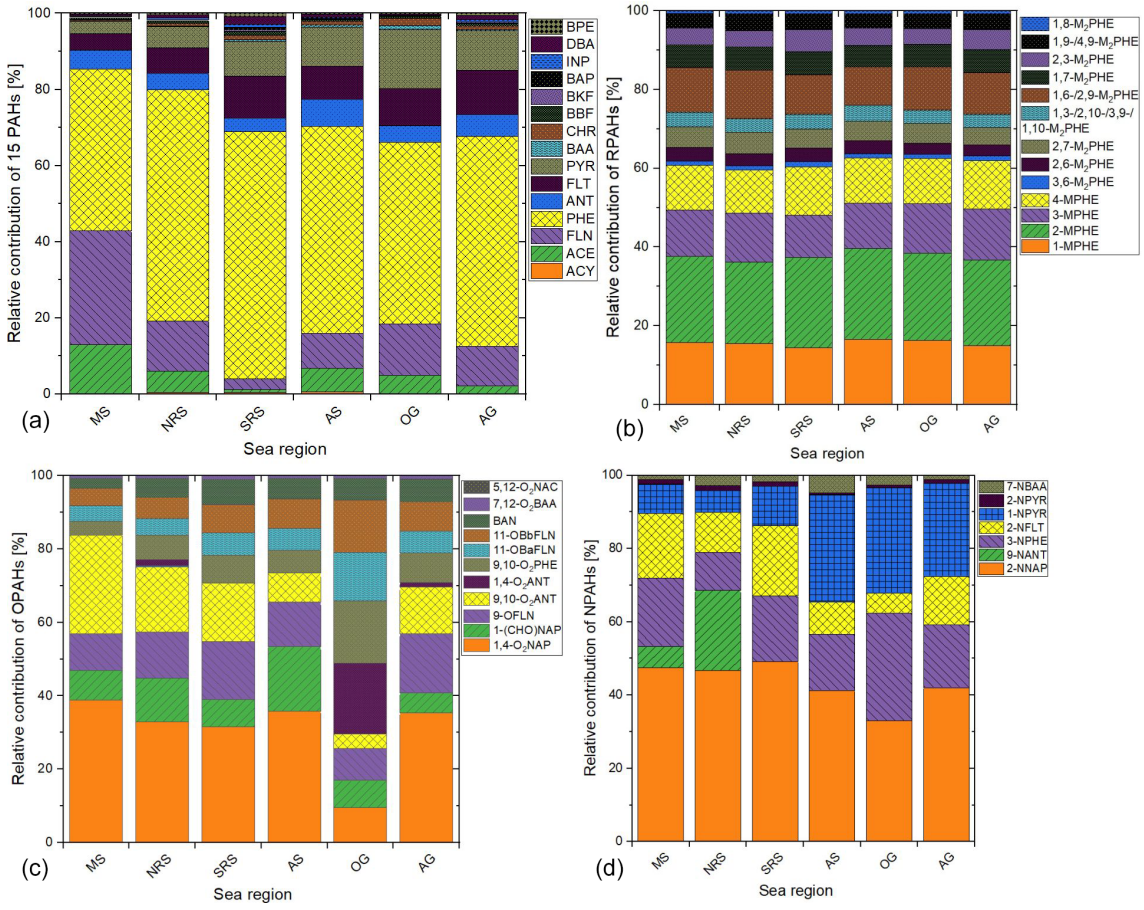

Figure 3. Relative amount of **(a)** 16 PAHs, **(b)** RPAHs, **(c)** OPAHs and **(d)** NPAHs across sea regions. MS: Mediterranean Sea; NRS: northern Red Sea; SRS: southern Red Sea; AS: Arabian Sea; OG: Gulf of Oman; and AG: Arabian Gulf. Full names of the substances are given in Sect. 2.3.1 and 2.3.2 and Tables 1 and S2. Only quantified species are included in legends.

an average contribution of 35 %, 22 % and 11 %, respectively. The high share of 9,10-O_2ANT and 9-OFLN was also found at several continental sites (Albinet et al., 2007, 2008; Li et al., 2015; Wei et al., 2015; Tomaz et al., 2016; Drotikova et al., 2020; Lammel et al., 2020; Jariyasopit et al., 2021; Nežiková et al., 2021). In several of these papers, 1,4-O_2NAP was not measured. Nežiková et al. (2021) and Jariyasopit et al. (2021) only found small relative amounts of 1,4-O_2NAP at the continental background site Košetice and in the Athabasca oil sands region in Canada, respectively. In contrast, Wei et al. (2015) and Lammel et al. (2020) found relatively high contributions to the total amount of OPAHs at urban sites in China and in the Czech Republic, respectively. Bandowe et al. (2014) observed higher concentrations of 1,4-O_2NAP in summer in $PM_{2.5}$ compared to the cold season, although the partitioning of the compound will be shifted to the gas phase in summer. This would lead to lower concentrations in summer since the degradation rates of most PACs are expected to be higher in the gas phase (Feilberg et al., 1999; Keyte et al., 2013). They hypothesised that 1,4-O_2NAP is significantly formed by secondary formation, as also shown by Kautzman et al. (2010) and Keyte et al. (2013). This can be supported by the low winter-to-summer ratio of 1,4-O_2NAP despite higher emissions in winter at Košetice (Nežiková et al., 2021). High secondary formation in plumes especially in the Mediterranean Sea and the Arabian Gulf (as explained in Sect. 3.3.4), as well as low reaction rates for the degradation of 1,4-O_2NAP compared to all other OPAHs (Table S2, Atkinson et al., 1989), might explain the high relative contribution of this quinone in our study. In addition, it needs to be considered that 1,4-O_2NAP is also emitted primarily (Nalin et al., 2016; Tomaz et al., 2017; Clergé et al., 2019). Except for the samples from the Gulf of Oman, 1,4-O_2NAP always had the highest contribution of 25 %–40 %. This quinone is frequently reported as having a high ability to produce reactive oxygen species (Charrier and Anastasio, 2012; Verma et al., 2015).

In the Gulf of Oman, the contribution from high-molecular-weight OPAHs (4-ring OPAHs) was higher compared to the other regions. The composition pattern of the samples from the Arabian Sea differed from the other samples because of a lower share of 9,10-O_2ANT and a higher

share of 1-(CHO)NAP. The same was true for the samples of the first leg in the Mediterranean Sea (see Table S16). 1-(CHO)NAP has been reported prominent among OPAHs from urban and other polluted sites but not generally (Albinet et al., 2007, 2008 (partly); Wei et al., 2015; Tomaz et al., 2016; Lammel et al., 2020 (in Kladno)).

3.2.4 NPAHs

Similar to the OPAHs, the regional differences in the NPAH composition pattern are more pronounced than the PAH and RPAH patterns. As illustrated in Fig. 3d, the most abundant NPAHs were 2-NNAP, 3-NPHE, 2-NFLT and 1-NPYR, with an average contribution of 45 %, 18 %, 15 % and 12 %, respectively. The contribution of 2-NNAP ranged between one-third and one-half in all regions. However, it was not detected above the LOQ in the gas phase of samples from the Arabian Sea. Due to the total detection frequency of > 30 %, the values were replaced by LOQ/2, which could lead to an overestimation in this case. A large fractional contribution of NNAPs, 3-NPHE and 2-NFLT was also found by Lammel et al. (2017) in the eastern Mediterranean Sea. At the continental site in the study from Lammel et al., as well as in other previous studies at continental sites, 2-NFLT, 9-NANT and 1-NNAP were the most abundant NPAHs (Bamford and Baker, 2003; Albinet et al., 2007, 2008; Tomaz et al., 2016; Drotikova et al., 2020; Lammel et al., 2020; Nežiková et al., 2021). In our study, 9-NANT only had a significant contribution in the northern Red Sea. We found only a few samples with 9-NANT > LOQ (LOQs in Table S7.1). The reason for the low contribution during the entire campaign might be the relatively high LOQ compared to other NPAHs (Table S7.1). In contrast to our campaign, several other studies found significant amounts of 1-NNAP in air samples at mid-latitude but continental sites (Bamford and Baker, 2003; Albinet et al., 2007, 2008; Tomaz et al., 2016; Drotikova et al., 2020; Lammel et al., 2020; Nežiková et al., 2021). The low contribution of 1-NNAP in air over the Mediterranean and around the Arabian Peninsula could also be due to the relatively high LOQ in PUFs (Table S7.1) or the photodegradation of 1-NNAP, which is faster than of 2-NNAP, as described by Feilberg et al. (1999). We hypothesise that the comparably low rate constants for the photodegradation as well as for the reaction with OH (Table S2, US EPA, 2019) are one reason for the high relative contribution of 2-NNAP. 2-NNAP is frequently detected in continental sites but mostly with lower relative contributions than 1-NNAP, 9-NANT and 2-NFLT (Bamford and Baker, 2003; Albinet et al., 2007, 2008; Tomaz et al., 2016; Drotikova et al., 2020; Lammel et al., 2020; Nežiková et al., 2021). Only at a remote site in Chile was 2-NNAP also found to have a very high relative contribution, which was explained by direct emissions or transport assuming a long atmospheric lifetime (Scipioni et al., 2012). The resistance to photochemical degradation can also be supported by the finding from Nežiková et al. (2021) that the relative contribution of 2-NNAP is higher in summer than in winter. However, this can also be due to different emission sources or stronger secondary formation in summer (Zhuo et al., 2017).

The fractional contribution of 1-NPYR is high in the Gulf of Oman and the Arabian Gulf. This can be explained by a significant amount of 1-NPYR in the exhaust of fossil fuel combustion (IARC, 2018; Zhao et al., 2015) and its high abundance near petrochemical industries (Caumo et al., 2018). It is used as a marker for primary emissions since it does not have significant secondary sources (Arey et al., 1986). The relatively short estimated lifetime of 1-NPYR in air due to photodegradation (Fan et al., 1996; Feilberg and Nielsen, 2000) and the small reaction rate with OH (Table S2, US EPA, 2019) could explain its low contribution in the Mediterranean Sea, since we sampled relatively aged air samples in that region. The relatively high contribution of 1-NPYR in the Arabian Sea might be due to bypassing ships (Table S18) as we found 1-NPYR highly abundant in the ship exhaust (Sect. 3.3.1). The high contribution of 1-NPYR in samples D40–42, in or close to the Gulf of Aden, is possibly due to pollution from coastal cities in the northeastern province of Somalia. The continental influence of these samples is also shown in the results of the PMF analysis (Fig. 4b). The large contribution of long-range-transported aerosols in the Mediterranean Sea is also illustrated by the high contribution of 2-NFLT, which is formed in secondary processes (Arey et al., 1986) and undergoing long-range transport on even a global basis (Wilson et al., 2020). The contribution of 2-NFLT is also high in the southern Red Sea, a region with minor influence of primary emissions but higher fraction of long-range-transported aerosols. 3-NPHE, which has primary (primary: Bamford et al., 2003; mainly primary: Zhuo et al., 2017) and secondary sources (secondary: Atkinson and Arey, 1994; Ringuet et al., 2012a; mainly secondary: Tomaz et al., 2017), has an almost similar contribution in all regions. This could be explained by various different sources or a long mean atmospheric lifetime.

3.3 Source apportionment

3.3.1 Sources of PAH derivatives by PMF

As shown in Figs. 4 and S4 as well as described in the Supplement (Sect. S2.4.1), the PMF analysis revealed five different source factors, namely fresh and aged shipping emissions, continental emissions, residual oil combustion and desert dust.

The PAHs, NPAHs and OPAHs in the air over the Mediterranean Sea and in the seas around the Arabian Peninsula are believed to originate primarily from fresh and aged shipping emissions. Fresh shipping emissions, mainly from the ship stack of our research vessel *Kommandor Iona*, were predominantly apparent during the first leg due to the prevailing wind direction. The model output and the filtering of possibly

stack-contaminated samples strongly agree. Samples filtered for stack contamination also show a contribution from fresh shipping emissions (e.g. samples D2, D3 from 26–28 June; D16–D23 from 14–22 July; and D26–D28 from 25–28 July). The stack filtering has rejected even a few samples without significant contribution from the factor (D9–D11 from 4–7 July). In contrast, a minor contribution to the factor of fresh shipping emissions was found in the Mediterranean Sea for samples around 30 August, which were not excluded by our filtering. This might be explained by fresh emissions from other ships close to the strait of Messina. Aged shipping emissions mainly contributed to air pollution in regions with congested marine routes such as the Suez Canal (4 July and 20–23 August 2017), the Bab al-Mandab Strait near Djibouti (16–17 July 2017) and the Strait of Hormuz, especially near Fujairah (26–28 July and 5–6 August 2017). The number of bypassing ships, potentially influencing the sampled air, based on the data from Celik et al. (2020), is given in Table S18.

Another important source of PAH derivatives was continental emissions. Based on the distribution of residence times of air masses during these sampling times, we could conclude that these emissions mainly came from Europe (especially received in the Mediterranean Sea but also in the Arabian Gulf), countries around the Arabian Gulf (mainly received there) and Egypt (mainly received in the northern Red Sea). Furthermore, the PACs originated from residual oil combustion. High factor contributions (Figs. 4b and S4b) in the period between 24 July and 6 August 2017 were linked to the samples collected in the Gulf of Oman and the Arabian Gulf and influenced by the emissions in the coastal areas and offshore (Fig. S3e and f), as also reported by Bourtsoukidis et al. (2019), Eger et al. (2019), Pfannerstill et al. (2019) and Wang et al. (2020). The source factor identified with minimum contributions of NPAH and OPAHs was desert dust. The finding of PAH derivatives in the factor desert dust could be explained by mixing of dust with other emissions sources such as continental pollution or shipping emissions. The concentration of the factor desert dust peaked primarily during a period of Sahara dust outbreaks (from 13–18 July 2017), while samples were collected over the Red Sea and over the western part of the Gulf of Aden (Fig. S3c and d, see also Eger et al., 2019). Dust emitted on the Arabian Peninsula is evident during the sail in the Gulf of Oman and the Arabian Gulf (24 July and 6 August 2017, Fig. S3d and e) but mixed with several other sources.

The contribution of the individual OPAHs and NPAHs can be seen in PMF group 2 in Figs. 4 and 5, showing the relative contributions of each factor to the concentration of each substance. All PACs targeted in the PMF run (group 2) had a significant contribution from fresh shipping emissions as their source. Moreover, by comparing several samples with a significant influence of the exhaust from the own stack (samples D16; 17; 20; 22; 23; 28; 37; 38; see Table S4 and Fig. S4) to the stack-filtered regional average concentrations, we could show that almost all detected PAHs, NPAHs and OPAHs were elevated in the samples with fresh shipping emissions (Table S17). 1-NPYR showed the highest ratio of contaminated to filtered samples among the NPAHs, while 11-OBaFLN and 1-(CHO)NAP had the highest ratio among the OPAHs. All targeted OPAHs showed a ratio higher than 1. For the NPAHs, only 2-NFLT was not elevated, except for a ratio of 5 in the Arabian Sea. 2-NFLT had been reported to be present in diesel particulate matter (Bamford et al., 2003; Zimmermann et al., 2012). However, this was explained by the gas-phase formation of 2-NFLT after emission during sample collection. Surprisingly, the concentration of 2-NPYR was significantly elevated in the fresh shipping emissions. This is unexpected, as 2-NPYR was reported absent in diesel exhaust (Bamford et al., 2003) and believed to be formed through secondary formation only (Finlayson-Pitts and Pitts, 1999; Wilson et al., 2020). Zhao et al. (2019, 2020) found significant amounts of 2-NPYR in ship exhaust gas depending on the fuel type and the engine loading. They report high emissions of this compound, especially with heavy fuel oil use and mainly under low engine speeds. The abundance of 2-NPYR was explained by secondary formation due to higher NO_x emissions and higher residence times during these conditions. The results from Zhao et al. (2019, 2020) and from our study suggest a very high formation rate of 2-NPYR. According to Keyte et al. (2013) and Wilson et al. (2020), the reaction rate constant of PYR with OH is 5 times higher for 2-NPYR compared to 2-NFLT but the yield of 2-NPYR is lower.

The large contribution of aged shipping emissions to the concentration of 2-NFLT and 2-NPYR (Fig. 5) illustrates the importance of secondary formation of these two NPAHs. In contrast, 1-NPYR is not abundant in the aged shipping emissions, showing that there is no significant secondary formation. It has been reported that 1-NPYR arises solely from primary emissions (Bezabeh et al., 2003; Reisen and Arey, 2005). The contribution of aged shipping emissions to the occurrence of 3-NPHE could either be explained by the higher atmospheric half-life of 79 h compared to 2-NFLT, 1-NPYR and 2-NPYR (Table S2, US EPA, 2019) or by secondary formation, as previously suggested (Tomaz et al., 2017). All detected OPAHs were abundant in the aged shipping emissions. Their abundance points to a long lifetime or formation in the atmosphere. The relative contributions of 11-OBaFLN, BAN and 7,12-O_2BAA were relatively small (Fig. 5). For 5,12-O_2NAC and 1,4-O_2NAP, the contribution of aged shipping emissions was higher. It was previously reported that from the measured OPAHs, 1,4-O_2NAP, 1-(CHO)NAP, 9-OFLN, 9,10-O_2ANT, 1,4-O_2ANT, 9,10-O_2PHE, 11-OBaFLN and 7,12-O_2BAA can be formed from the reaction of parent-PAHs with oxidants (Helmig and Harger, 1994; Perraudin et al., 2007; Wang et al., 2007; Gao et al., 2009; Ringuet et al., 2012a; Keyte et al., 2013; Dang et al., 2015). Based on the previous findings from literature and the results of the PM factor "aged shipping emissions", a contribution

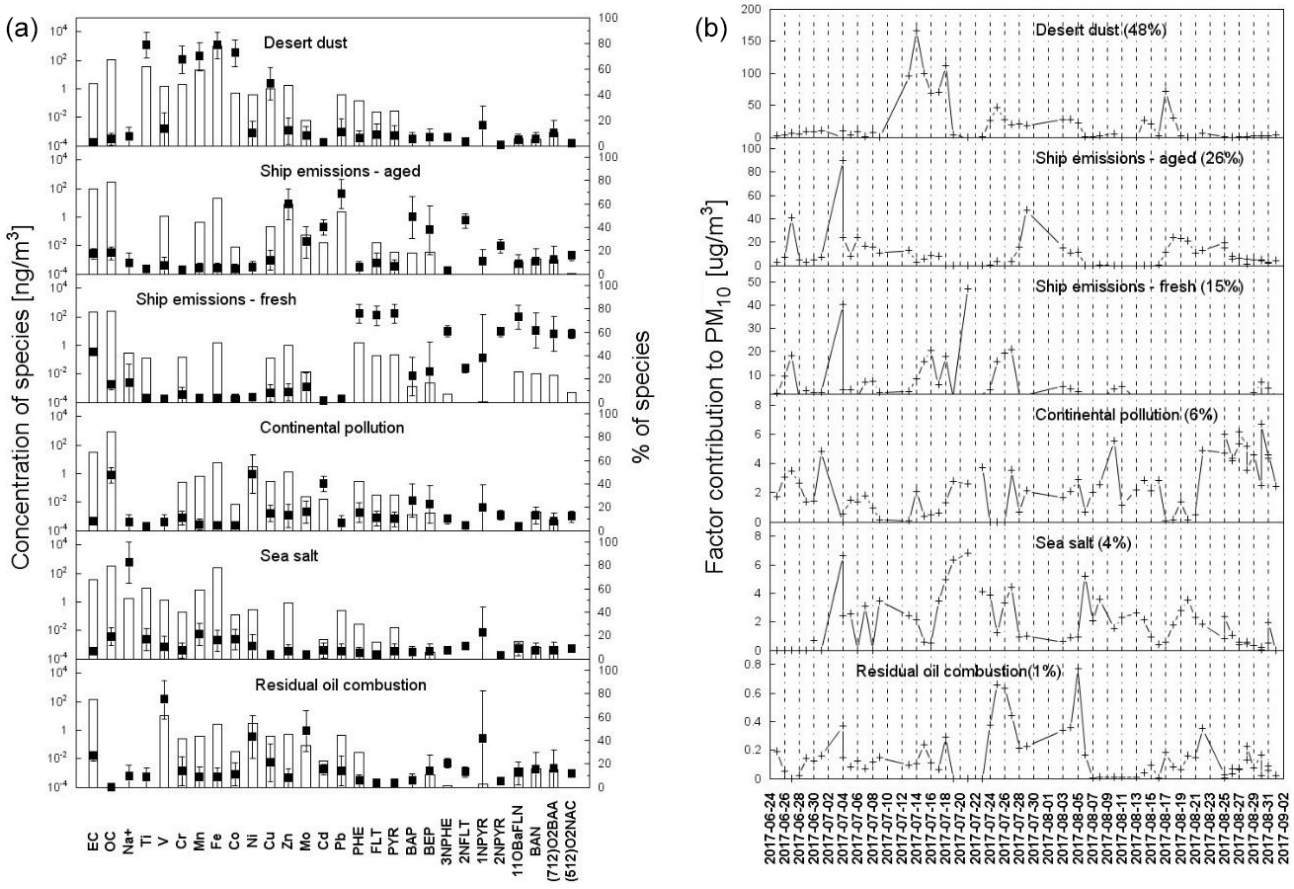

Figure 4. PMF group 2. **(a)** Factor profiles (bars: concentration of the species, black squares: percentage of the species explained, box: displacement (DISP) average, and whiskers: DISP max and DISP min) and **(b)** time series of factor contributions to sample composition.

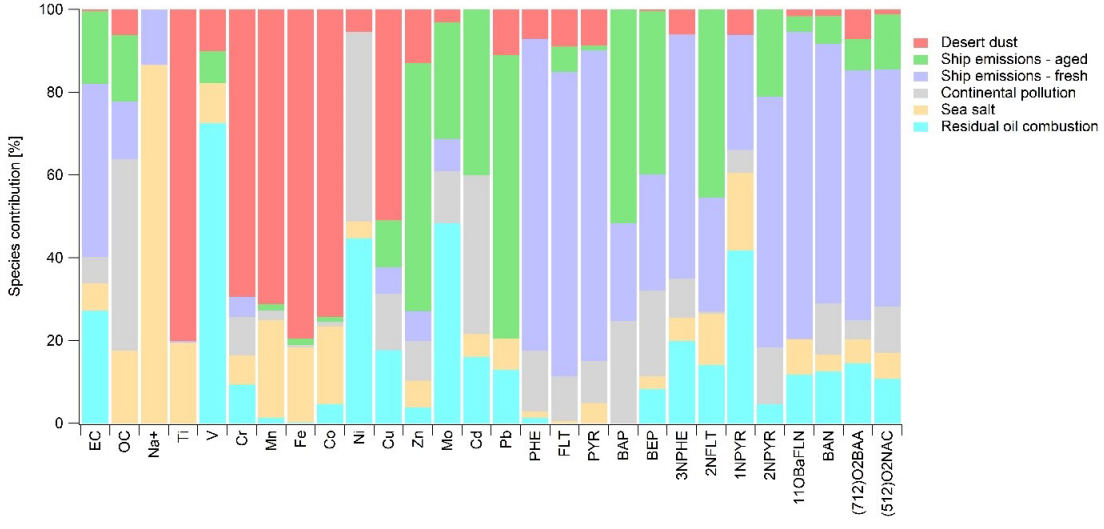

Figure 5. Relative contribution of the five factors resolved by PMF to the concentration of each substance in PMF group 2.

from secondary formation to the burden of 1,4-O_2NAP and 7,12-O_2BAA is likely, in addition to the known secondarily formed substances 2-NPYR and 2-NFLT. Since BAN and 11-OBaFLN have not been found as secondary formation products but are highly abundant in primary emissions (Albinet et al., 2007; Ringuet et al., 2012a; Clergé et al., 2019), we hypothesise that their contribution to aged shipping emissions is only due to their atmospheric lifetime. Since the primary emitted 1-NPYR is not abundant in aged shipping emissions, it shows that BAN and 11-OBaFLN have a higher atmospheric lifetime than 1-NPYR. Since the estimated lifetime due to oxidation by OH is higher for 1-NPYR than for the two OPAHs (Table S2, US EPA, 2019), degradation of 1-NPYR is expected to be governed by photodegradation (Feilberg and Nielsen, 2000), as already mentioned in Sect. 3.2.4. Since there are not many data in the literature about 5,12-O_2NAC, its abundance in aged shipping emissions can either be due to high atmospheric lifetime or secondary formation.

1-NPYR and 3-NPHE seem to be good tracers for oil combustion, hence the correlation with emissions from the petrochemical industry in the Gulf of Oman and the Arabian Gulf. 1-NPYR and 3-NPHE are known to be emitted during combustion of oil (Streibel et al., 2017). In addition, all OPAHs included in the PMF, except for 1,4-O_2NAP, originated directly or secondarily from residual oil combustion.

Except for 11-OBaFLN, all considered PAHs, OPAHs and NPAHs are partly from continental pollution (Fig. 4a). The abundance of these air pollutants in continental pollution, including 11-OBaFLN, has been shown in many studies (Bamford and Baker, 2003; Albinet et al., 2007, 2008; Wei et al., 2015; Tomaz et al., 2016; Drotikova et al., 2020; Lammel et al., 2020; Nežiková et al., 2021). The missing contribution of continental pollution to the concentration of 11-OBaFLN might be because of its comparably low atmospheric half-life due to degradation by OH (Table S2, US EPA, 2019). Continental pollution was highly abundant in the Mediterranean Sea (Fig. 4b), where we found the highest concentrations of the OH radical of the entire AQABA campaign. 1,4-O_2NAP has a comparably high contribution of approx. 50 % by this factor. As explained in Sect. 3.2.3, this might be explained by high relative concentrations at the source, high atmospheric lifetime and secondary formation during the transport of the air to the sampler. In contrast, 1,4-O_2NAP seems to be significantly less abundant in pollution from the combustion of residual oil (Fig. 4a) and marine diesel (Table S17). However, more research is needed to evaluate this aspect in more detail. All PACs are abundant in desert dust, except for BAP and 2-NPYR. The presence of PAHs and PAH derivatives, especially 1-NPYR and 1,4-O_2NAP in the factor desert dust (Fig. 4a), may indicate co-emissions of dust and PACs in the region (e.g. close to onshore industries).

3.3.2 Source attribution by PAHs and alkylated PAHs

The ratio of the particulate concentration of BAP to BAP + BEP is often used as a marker for the ageing of atmospheric particles since photodegradation of BAP is faster than of BEP (Tobiszewski and Namieśnik, 2012). A concentration ratio BAP/(BAP + BEP) of less than 0.5 indicates photochemically aged aerosols. The ratio was below 0.5 in all regions except for the Arabian Sea, showing a ratio of $\approx$ 0.5 (see Fig. S5). The somewhat elevated ratio in the Arabian Sea might be caused by local ship plumes (for number of encounters see Table S18; identification based on Celik et al., 2020) and other offshore emissions, which contributed to the mostly long-range-transported and aged air pollution in the region. This is also supported by Bourtsoukidis et al. (2019) in the study of non-methane hydrocarbons during the AQABA campaign.

The relatively low ratios in all other regions might be explained by the low number of primary sources of air pollutants at sea except for ship traffic and some emissions from the offshore oil and gas industry. Thus, the pollution from urban and industrial areas, which are located mostly on the coast, is already slightly aged when reaching the sampler on the ship, depending on the proximity to the emission sources. This could also be the explanation why the second highest regional average values were found in the southern and the northern Red Sea, receiving the emissions from the nearby coast as well as from the intense ship traffic in the region. The lowest regional average BAP/(BAP + BEP) values were detected in the Gulf of Oman and the Arabian Gulf. Air mass histories of sample D33 showed that a significant amount of aerosols came from less populated areas of Iran with a low amount of primary emissions (Fig. S3f, Wang et al., 2020). The results in the Mediterranean Sea can be divided into the first leg, with a lower BAP/(BAP + BEP) ratio due to the prevalent westerly winds bringing aged air from Africa and from the sea, and the second leg, with higher ratios due to pollution from close European coastal areas and islands. Samples D58 and D49–52, close to Sicily and the Greek islands (coordinates in Table S1), respectively, showed the highest BAP/(BAP + BEP) ratios.

The RPAHs could not be included in any multivariate analysis since the RPAH sampling followed another sampling protocol than the PAHs, OPAHs and NPAHs, with only very few similar sampling times. The ratio of ΣMPHE/PHE < 1 indicates pyrogenic origin of PAHs for most days in the Red Sea, while a ratio of ΣMPHE/PHE > 1 indicates petrogenic origin, i.e. from unburned fuel (Gogou et al., 1996), which occurred during the period from the 8–9 July 2017 in the northern Red Sea. Findings by Bourtsoukidis et al. (2020) could tentatively provide an explanation for the high ratio of ΣMPHE/PHE observed, namely degassing from the Red Sea Deep water. The ratio of the sum of the four MPHE homologues to PHE (ΣMPHE/PHE) and the ratio 1,7-M_2PHE/(1,7-M_2PHE + 2,6-M_2PHE) are given in Ta-

ble S14. The distribution patterns and the concentration ratio 1,7-M_2PHE/(1,7-M_2PHE + 2,6-M_2PHE) may be interpreted by considering the emission sources of these compounds. Bläsing et al. (2016) characterised and compared patterns of alkylated PAHs in gaseous and particulate emissions from road traffic (diesel), domestic heating, inland navigation vessels (INVs) and ocean-going vessels (OGVs). The ratio of 1,7-M_2PHE/(1,7-M_2PHE + 2,6-M_2PHE) was used to distinguish the above-mentioned emissions. Thus, the ratio of 1,7-M_2PHE/(1,7-M_2PHE + 2,6-M_2PHE) for INVs (0.37–0.62) is comparable with that from road traffic and domestic heating. In comparison, 1,7-M_2PHE/(1,7-M_2PHE + 2,6-M_2PHE) for marine oil combustion (as used for OGVs) was 0.68 (Budzinski et al., 1995). In the present study, the calculated average ratios were 0.63 (first leg) and 0.66 (second leg) for the Mediterranean, 0.64 and 0.62 for the Red Sea, 0.66 and 0.71 for the Oman Gulf, 0.73 and 0.67 for the Arabian Gulf, respectively, and 0.61 (second leg) for the Arabian Sea. The calculated values for 1,7-M_2PHE/(1,7-M_2PHE+2,6-M_2PHE) in the present study are within the range 0.60–0.70, proposed by Bläsing et al. (2016) as an indicator for the emissions of OGVs.

3.3.3 Source attribution by NPAHs and OPAHs

Similar to the ratio of BAP/(BAP + BEP), the ratio of 2-NFLT/1-NPYR can indicate the photochemical age of aerosols. A ratio < 5 shows the predominance of combustion sources, while a higher ratio indicates photochemically aged aerosols (Ciccioli et al., 1996). As illustrated in Fig. 6a, the highest regional average ratio of 2-NFLT/1-NPYR but also with the highest standard deviation was found over the Mediterranean Sea, followed by the southern and the northern Red Sea. The average 2-NFLT/1-NPYR ratio in air sampled over the Mediterranean Sea and over the northern Red Sea were significantly higher ($p < 0.05$, Student's t test) than in the air from Arabian Sea and the Gulf of Oman, respectively. Although the ratio of BAP to BEP suggests aged aerosols in several samples (Sect. 3.2.2), the ratio was higher than 5 in only two samples (D1 and D58, collected over the Mediterranean Sea, coordinates in Table S1). In polluted air near the coast (e.g. as found in the Red Sea and at the beginning and the end of the campaign in the Mediterranean Sea) and in plumes (in samples D1, D30, D48 and D58, coordinates in Table S1), the 2-NFLT/1-NPYR ratio was high.

The reason for the low incidence of high ratios could be that the concentrations of atmospheric oxidants OH and NO_3 radicals as well as NO_2 in some sea regions during the campaign were low (Bourtsoukidis et al., 2019; Tadic et al., 2020; Friedrich et al., 2021). The difference might be caused by different oxidants being responsible for the degradation of BAP and formation of 2-NFLT. BAP, which is predominantly in the particulate phase, is mainly degraded by heterogeneous reaction with ozone (Shiraiwa et al., 2009), while 2-NFLT is mainly formed by homogeneous reaction of FLT with OH or NO_3 (Atkinson and Arey, 1994; Reisen and Arey, 2005) and subsequent reaction with NO_2. Ozone concentrations varied between 20 ppbv (in the Arabian Sea) and 150 ppbv (in the Arabian Gulf), while NO_x showed a higher variation (from 50 pptv to more than 10 ppbv) (Tadic et al., 2020; Friedrich et al., 2021). The highest NO_x mixing ratios were found in the northern Red Sea and the Gulf region, especially close to the Suez Canal, Kuwait and Fujairah (Tadic et al., 2020; Friedrich et al., 2021). NO_2 concentrations are generally significantly smaller in the marine environment than on land, as shown by satellite data (Roşu et al., 2019) due to the short lifetime (Schaub et al., 2007; Shah et al., 2020) and missing sources for NO_x at sea except for ship traffic and the offshore oil and gas industry. Friedrich et al. (2021) calculated NO_2 lifetimes of less than 6 h during the AQABA campaign, which means that land-based NO_x emissions will be degraded before reaching the sampler for several samples. However, NO_2 is crucial for the formation of 2-NFLT competing with O_2 to either form NPAHs or OPAHs, respectively (Kamens et al., 1994; Finlayson-Pitts and Pitts, 1999; Atkinson and Arey, 2007).

The ratio of 2-NFLT/1-NPYR can rise during transport of the pollutants. However, the formation of 2-NFLT slows down or stops, probably due to low concentrations of the parent-PAH (FLT), the atmospheric oxidants OH and NO_3 or NO_2 since formation of 2-NFLT depends on these reactants (Wilson et al., 2020). This was also shown by Lammel et al. (2017), who found much larger yields of 2-NFLT and 2-NPYR in the marine background with urban influence compared to the marine background without significant pollution sources.

In contrast to the regions with polluted air, a low ratio was observed in air over the Arabian Sea and in the parts of the Mediterranean Sea far from the coast. The average ratio in the Arabian Sea was only 0.36. This points to primary sources (as indicated in Sect. 3.3.2) and/or very low NO_2 concentrations in the sampled air masses as shown by Friedrich et al. (2021). When secondary formation far away from sources is not significant anymore, the differences in characteristic time for chemical (which is primarily photolysis) and physical sinks (which is primarily particle deposition) determine the ratio of 2-NFLT/1-NPYR. One influencing factor might be the difference in deposition velocity of the two compounds due to the different particulate fractions, which is lower for 2-NFLT (not shown; gas–particle partitioning is studied in a separate paper). A lower particulate mass fraction of 2-NFLT might lead to a slower deposition of this compound compared to 1-NPYR, which would lead to higher ratios. In contrast, a lower ratio would be the result of the faster degradation of 2-NFLT by OH and ozone compared to the degradation of 1-NPYR (Table S2, US EPA, 2019). In contrast, 1-NPYR is probably more prone to photodegradation, although the photodegradation rates strongly depend on the aerosol composition (Feilberg and Nielsen, 2000). The removal and degradation rates are reported to

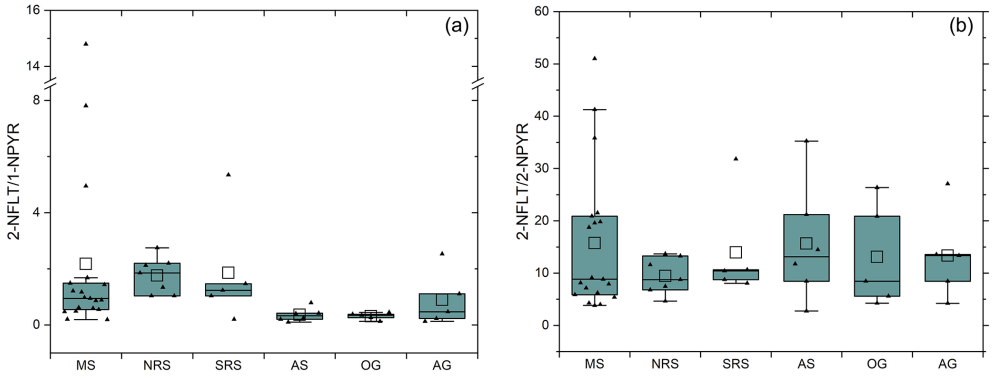

Figure 6. Box-and-whisker plot of the ratios **(a)** 2-NFLT/1-NPYR and **(b)** 2-NFLT/2-NPYR across sea regions. MS: Mediterranean Sea; NRS: northern Red Sea; SRS: southern Red Sea; AS: Arabian Sea; OG: Gulf of Oman; and AG: Arabian Gulf. Empty square: mean value. Filled grey triangles: measurement points. Box with additional borders: interquartile range (IQR) bound by the 75th and 25th percentile and range of 1.5 IQR. Horizontal line: median).

be approximately similar (Kamens et al., 1994; Fan et al., 1996; Feilberg and Nielsen, 2000; Albinet et al., 2008). However, this may not be the case in this study due to exceptionally low particulate mass fractions of the PACs due to the high temperature and the low EC and OC concentrations in the aerosols (Table S15). If degradation of 2-NFLT plays a larger role in the investigated regions, the ratio of 2-NFLT/1-NPYR would decrease with time, when there is no formation of 2-NFLT. This might be another explanation for the low 2-NFLT/1-NPYR ratios in some sea regions. However, more research is needed on the exact kinetics influencing the ratio, especially the photolysis rate coefficients. At continental sites, the ratio of 2-NFLT/1-NPYR mostly increases with distance to the emission source due to the significant formation of 2-NFLT (Ciccioli et al., 1996; Nežiková et al., 2021).

Since 2-NPYR is almost entirely formed by the reaction of PYR with OH radicals during daytime, while 2-NFLT can be formed by daytime reaction with OH as well as by nighttime reaction with NO_3, the ratio of 2-NFLT/2-NPYR can reveal the predominant formation pathway of NPAHs (Feilberg et al., 2001; Bamford and Baker, 2003). The main formation pathway during the campaign was the OH-radical-initiated formation, since the average concentration ratio of 2-NFLT/2-NPYR was 15.1 ± 11.6. This is close to a ratio of 5–10, suggesting the predominant formation of NPAHs by OH radicals but far from a ratio of > 100, which would indicate reactions mainly involving the NO_3 radical. This finding is similar to previous observations in the marine environment, i.e. the Japanese and Mediterranean seas (Tang et al., 2014; Lammel et al., 2017).

As illustrated in Fig. 6b, the lowest average ratio (9.5) was found in the northern Red Sea, while the ratio of 15.8 (first leg: 22.3; second leg: 13.4) in the Mediterranean Sea was the highest regional average value. The high value in the Mediterranean Sea during the first leg was due to two exceptionally high values in samples D1 and D5 (coordinates in Table S1). The formation of these NPAHs will be largely determined by the accumulated night-time NO_2 and the actinic flux during the day; the air mass had been exposed to prior sampling. For example, samples D52 and D56 had relatively high ratios since the aerosols had picked up NO_x emissions from the urban areas of Athens and Istanbul (D52) or Rome and Naples (D56) in a previous night, which can be converted to the NO_3 radical by the reaction with ozone, whereas samples D50 and D54, which had not picked up NO_x emissions from particular source areas within ≈ 48 h, did not show a high 2-NFLT/2-NPYR ratio.

3.3.4 PAHs and derivatives in photochemically aged pollution

A high ratio of the secondarily formed PAH derivatives 2-NPYR and 2-NFLT (Arey et al., 1986; Bamford and Baker, 2003; Reisen and Arey, 2005) to their parent PAHs PYR and FLT, respectively, indicates long-range-transported aerosols with a significant concentration of the atmospheric oxidants OH and NO_3 as well as NO_2. Similar to the ratio of 2-NFLT/1-NPYR, the highest ratios were observed in air over the Mediterranean Sea (especially during the first leg in aged aerosols). We determined the highest ratios in sample D1 at the beginning of the campaign close to Sardinia and Sicily. Another high ratio was found in sample D30 in the Arabian Gulf. As already revealed by Wang et al. (2020), photochemically aged air reached the ship from the first night of the first leg in the Arabian Gulf (28 July 2017, 16:00 UTC) until the 30 July 2017 at 00:00 UTC (see air mass histories in Fig. 7a), as evidenced by high mixing ratios of some carbonyl compounds such as acetone. After that, the air was dominated by fresh emissions, while approaching Kuwait. According to the distribution of residence times of air masses, the air arrived from northwest with influence of several oil fields and refineries in that region (Figs. 7b and S3f; Bourt-

soukidis et al., 2019; Pfannerstill et al., 2019; Wang et al., 2020). Thus, the samples from the first leg in the Arabian Gulf were affected by fresh emissions as well as photochemically aged air. Apart from 2-NFLT/FLT and 2-NPYR/PYR, several other PAH derivatives to parent-PAH concentration ratios (e.g. 9-OFLN/FLN and 9,10-O_2ANT/ANT) were also elevated in sample D30 (coordinates in Table S1), showing the high contribution of photochemically aged air. In addition, the results indicate that these PAH derivatives are secondarily formed or significantly more slowly degraded and deposited than their parent PAH.

Another sample with a high ratio of secondarily formed NPAHs is sample D48 in the northern Red Sea nearby the Suez Canal. Similar to the first night in the Arabian Gulf, Wang et al. (2020) determined a high OH exposure during the first night in the Gulf of Suez (22–23 August 2017) accompanied by a high mixing ratio of acetone. The finding that aerosols sampled between the 22 and 23 August 2017 (D48) were atmospherically aged is supported the high PAH derivative / parent PAH ratios (e.g. of 2-NFLT/FLT, 2-NPYR/PYR, 7-NBAA/BAA, and 9,10-O_2ANT/ANT). The enhanced formation of NPAHs and OPAHs from atmospheric reactions in this area is commensurate with high concentrations of NO_2 and comparably high production rates of the NO_3 radical in this sea region, as reported by Eger et al. (2019). In addition, sample D48 (coordinates in Table S1) is also affected by primary emissions, e.g. from oil refineries and ship traffic (Bourtsoukidis et al., 2019). This is supported by the PMF, suggesting aged shipping emissions as well as continental pollution as the major sources.

Generally, low and high NPAH/PAH and OPAH/PAH ratios coincided with NO_x and radical availabilities. The highest concentrations of PAHs (D54) as well as of NPAHs and OPAHs (D58) were found in air masses carrying continental pollution, sampled in the Mediterranean Sea (from southeast Europe, covering major urban areas including Thessaloniki and Istanbul as well as from Sicily, Corsica, Sardinia and parts of continental Italy, respectively; Fig. 7c and d). While night-time sample D54 corresponded to low NO_x and low OH and NO_3 radical concentrations, 24 h sample D58 corresponded to high OH and NO_x concentrations (Tadic et al., 2020; Friedrich et al., 2021).

We found significant positive correlations ($p < 0.05$, Student's t test) of 9-OFLN ($r = 0.33$), 1-(CHO)NAP ($r = 0.41$), 7,12-O_2BAA ($r = 0.83$), 2-NNAP ($r = 0.46$) and 3-NPHE ($r = 0.44$) with the ratio of 2-NFLT/1-NPYR, which is typically used as an indicator for the contribution of PAH derivatives formed from oxidative reactions. This supports the perception that 9-OFLN, 1-(CHO)NAP, 7,12-O_2BAA and 3-NPHE have photochemical sources apart from primary. Laboratory studies showed that 7,12-O_2BAA is formed in heterogeneous reactions of BAA with O_3 or with O_3 and NO_2 (Gao et al., 2009; Ringuet et al., 2012a, b). The formation of 7,12-O_2BAA from the photochemical reaction of BAA has also been reported by laboratory studies (Jang and McDow, 1997; Shen et al., 2007). Lin et al. (2015) also found field evidence for significant secondary formation of 3-NPHE and 7-NBAA. Tomaz et al. (2017) even suggested 3-NPHE to be used as a marker for secondary formation from PHE. 1-(CHO)NAP was already reported to be secondarily formed by ozonolysis from ACY, 1-methylnaphthalene and possibly other precursors within hours (Dang et al., 2015). These indications of photochemical sources are supported by PCA: the PCA score plot shows the ratios 2-NFLT/1-NPYR and 2-NFLT/FLT as indicative of secondary formation clustered with the parent-daughter ratios 7,12-O_2BAA/BAA and 7-NBAA/BAA. The ratio BAP/(BAP + BEP), which points to aged air samples, is clustered with 2-NPYR/PYR and 2-NNAP and close to 2-NPYR and the first cluster, indicating secondary formation of 2-NPYR (as known in the literature) and 2-NNAP. For 9-OFLN, 1-(CHO)NAP and 3-NPHE, the PCA did not reveal significant secondary formation.

3.4 Mass size distributions

The highest concentrations of PAHs, OPAHs and NPAHs are found in the sub-micrometre fraction of particulate matter, PM_1, i.e. 58 %, 89 % and 93 % of PAHs, OPAHs and NPAHs, respectively. For 1-NPYR and 2-NFLT the fractions were 92 % and 83 % in the Mediterranean Sea, while previously 68 % and 86 %, respectively, were reported (Lammel et al., 2017). The finding has two main implications. First, due to the low share of pollutants in particles > 1 µm, deposition lifetime against wet and especially against dry particle deposition is long (Pryor et al., 2008; Škrdlíková et al., 2011). Similar shares of OPAHs and NPAHs in PM_1 had been reported from urban sites (eastern Mediterranean and central Europe; Kitanovski et al., 2020). Second, a higher share in the ultrafine particle fraction might lead to higher adverse health effects since these ultrafine particles can penetrate deeper into the lung than bigger particles (Hussain et al., 2011). The result suggests a higher risk (assuming same toxicity) for PAH derivatives since the higher relative amount of OPAHs and NPAHs in the ultrafine fraction can reach deeper into the lung.

Figure 8 shows the campaign average mass size distributions (MSDs) of the PAHs and PAH derivatives. The MSDs of PAHs, NPAHs and OPAHs are mainly unimodal given the coarse size resolution of the impactor with six size ranges within PM_{10}. The maximum was found in particles with an aerodynamic diameter < 0.49 µm. For the sum of PAHs, four samples showed an apparently unimodal distribution with a maximum at a particle diameter of 0.49–0.95 µm in the accumulation mode instead of the lowest particle size. In addition, three samples (two in the Arabian Gulf and one in the Arabian Sea) showed a bimodal distribution with maxima in particles with an aerodynamic diameter < 0.49 µm and 0.95–1.5 µm. For the sum of NPAHs, only one sample (in the Mediterranean Sea) showed an apparently unimodal distribution with a maximum in another aerodynamic particle di-

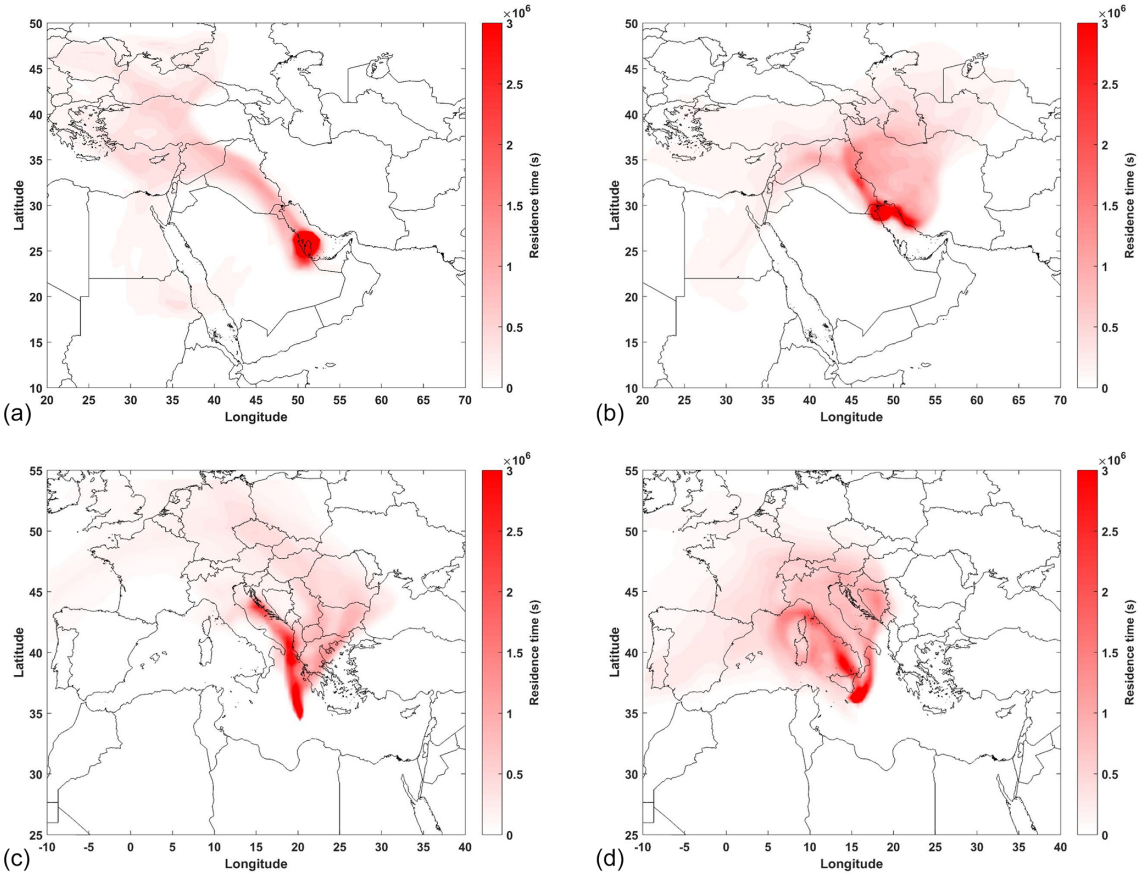

Figure 7. Distribution of residence times of air masses received in the Arabian Gulf: **(a)** D30 (29–30 July 2017), **(b)** D31 (3–4 August 2017) and the Mediterranean Sea: **(c)** D54–55 (27–28 August 2017) and **(d)** D58 (29–30 August 2017) using FLEXPART Lagrangian particle dispersion model samples.

ameter range than $< 0.49\,\mu m$ (0.49–0.95 µm). Since we did not resolve the $< 0.49\,\mu m$ size fraction, more modes in the sub-micrometre fraction, as found by di Filippo et al. (2010), cannot be excluded.

The ratio between the concentrations in particles $< 0.49\,\mu m$ compared to the concentrations in coarse-mode PM particles is greater for high-molecular-weight PACs compared to low-molecular-weight PACs (Fig. S7a and b) and higher for PAH derivatives compared to the parent-PAHs (Fig. S7c, d and e). This can be explained by the lower vapour pressure of PAH derivatives and high-molecular-weight PAHs compared to the parent-PAHs and low-molecular-weight PAHs. Compounds with lower vapour pressure are less subject to redistribution across particles sizes during transport (Degrendele et al., 2014). The process of redistribution is more effective in causing the pollutants to reach higher particle size fractions than the process of coagulation of particles to form larger particles, which would transfer low vapour pressure PACs to bigger particle size fractions. For PAHs, the mass median diameter (MMD) is significantly positively correlated with the subcooled liquid vapour pressure ($r = 0.54$, $p < 0.05$). The same is true for the NPAHs and OPAHs ($r = 0.98$, $p < 0.05$). The latter correlation is strongly biased by the high MMD of 1-(CHO)NAP. 1-(CHO)NAP was the only PAH derivative with relatively high vapour pressure which was quantified on the filters regularly. MMDs of the targeted substances are shown with their subcooled liquid vapour pressures in Fig. S9 (plotting all PACs with a detection frequency of $> 30\,\%$ in the impactor samples). It is striking that the MMD increases with increasing vapour pressure, but that dependence differs between PAHs and PAH derivatives, with the lower MMDs at the same vapour pressure for the latter. Semivolatile compounds are subject to redistribution across the size spectrum of aerosols during transport, which could be suppressed by specifically high affinity to the matrix of mode(s). The higher MMD diameter of PAHs indicates that high affinity of PAHs to BC (or EC; see, for example, Lohmann and Lammel, 2004) was not significant. BC (or EC) was concentrated in sub-micrometre particles (Fig. S8). This is not surprising in aerosols of which chemical compositions are dominated by sea salt and mineral dust. It seems that NPAHs and OPAHs

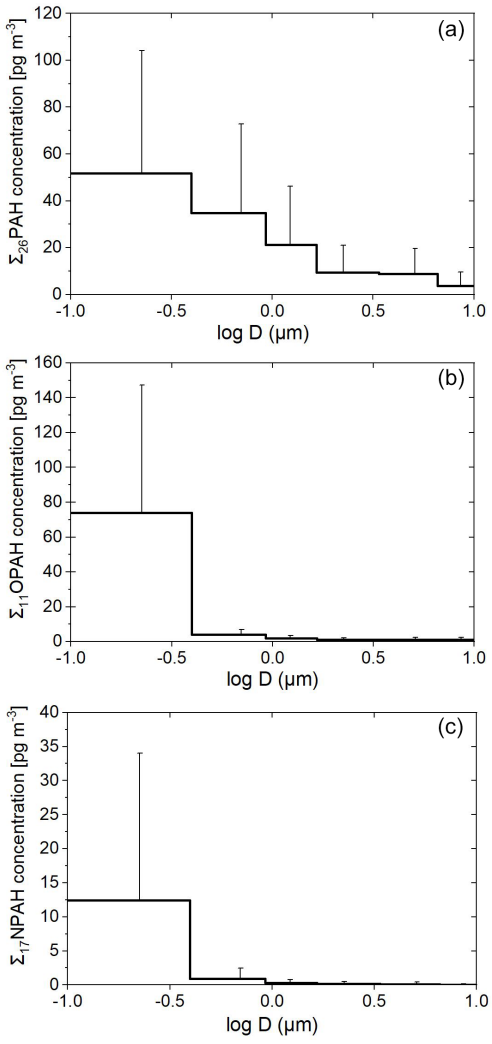

Figure 8. Campaign average mass size distributions (MSDs) of **(a)** $\sum_{26}$PAHs, **(b)** $\sum_{11}$OPAHs and **(c)** $\sum_{17}$NPAHs during the campaign, including standard deviation as error bars.

were less subject to redistribution than PAHs, possibly related to specific affinity to particles < 0.49 µm (Figs. 8, S7). Different mass size distributions between PAHs and PAH derivatives despite similar vapour pressures were reported from polluted rural environments and are explained by differences in the chemical affinity of the PACs to the PM matrix (Albinet et al., 2008). The NPAHs generally had a low concentration in our study, and most low-molecular-weight PACs were not abundant in PM since these substances are preferable in the gas phase. The campaign-average MMDs of the target compounds are shown in Table S19. As shown by Gao et al. (2019), the MSDs influence the dry-deposition velocities since coarse mode particles have a higher dry-deposition velocity than the particles in the fine particle fraction.

Since the process of redistribution depends on time, a shift of the MMD to larger particles sizes is found for aged aerosols (see exemplary Fig. S10). For instance, Lammel et al. (2017) found two maxima for the 4-ring PAHs at a marine background site (same cascade impactor as the one used in this study). The second maximum was explained by aged aerosols at the marine site. The samples showing a maximum of the sum of PAHs at higher particle diameters in our study can also be attributed to aged aerosols (aged samples C6 and C7 in Arabian Gulf; C27, C28 in Mediterranean Sea without close primary emission sources; C22 in very clean air over the Arabian Sea, C24 in southern Red Sea possibly because of Saharan dust).

For compounds with similar vapour pressures and polarity (or sorption to the PM matrix), differences in the MSDs could point to a different origin and/or time elapsed since release or formation of the compounds. The relative amount of the primarily emitted 1-NPYR in the fraction with a particle size of < 0.49 µm was higher and the MMD lower than of the secondarily formed 2-NFLT and 2-NPYR. This is also reflected by the ratio 2-NFLT/1-NPYR, indicative of the relative amount of secondarily formed PACs, which was highest in the accumulation mode (0.95–1.5 µm). This is in contrast to the findings of Ringuet et al. (2012b), who observed the highest ratios in the finest particle fraction, attributed to condensation of secondarily formed 2-NFLT to the aerosol surface, of which size distribution peaked in the finest fraction. Albinet et al. (2008) did not find an influence of primary or secondary origin of the PAH derivatives on their mass size distributions at polluted rural sites. One reason for the difference could be the lower relative amount of ultrafine particles in the marine atmosphere due to fewer primary sources and less new particle formation as compared to the polluted continental environment (Seinfeld and Pandis, 2016). However, even in a cloud-free atmosphere, the uncontrolled influencing parameters are too numerous, and more process-oriented studies would be needed to elucidate individual PAH derivatives' MSDs.

4 Conclusions

For the first time, PAHs and their derivatives were measured in the marine environment around the entire Arabian Peninsula in a comprehensive ship campaign. The atmospheric average concentrations of $\sum_{26}$PAHs, $\sum_{19}$RPAHs, $\sum_{11}$OPAHs and $\sum_{17}$NPAHs in the gas and particulate phase were 2.99 ± 3.35 ng m^{-3}, 0.83 ± 0.87 ng m^{-3}, 0.24 ± 0.25 ng m^{-3} and 4.34 ± 7.37 pg m^{-3}, respectively. The lowest burden of all targeted pollutant classes was observed in the Arabian Sea, with concentrations among the lowest ever reported, followed by the southern Red Sea. The highest average concentrations of the PAHs and the OPAHs were detected in the Mediterranean Sea, while the NPAHs were most abundant in the Arabian Gulf. It was observed that the regional differ-

ences in the composition patterns of the NPAHs and OPAHs were more pronounced than those of the PAHs and RPAHs. 1,4-O_2NAP, 9-OFLN and 9,10-O_2ANT were the most abundant OPAHs. The NPAH composition pattern was dominated by a high contribution of 2-NNAP, followed by 1-NPYR, which was highly abundant in the Gulf region. Photochemical formation of 2-NFLT, 2-NPYR, 2-NNAP, 3-NPHE, 7-NBAA, 1-(CHO)NAP, 9-OFLN and 7,12-O_2BAA was indicated, while for 1-NPYR, 11-OBaFLN, 11-OBbFLN, BAN and 5,12-O_2NAC secondary sources, it was not significant.

Source apportionment showed that the PAHs and their nitrated and oxygenated derivatives mainly originated from fresh and aged shipping emissions. All OPAHs and NPAHs except 2-NFLT, which were frequently detected during the campaign, showed elevated concentrations in fresh shipping emissions. 1-NPYR among the NPAHs and 11-OBaFLN and 1-(CHO)NAP among the OPAHs showed the highest relative increase in their concentration. In contrast, 2-NFLT and 2-NPYR were highly abundant in aged shipping emissions due to secondary formation. 1-NPYR, 3-NPHE and several OPAHs had a significant contribution from residual oil combustion. PAH derivatives were clearly enriched in long-range-transported plumes from polluted regions in Egypt, the Arabian Gulf, and southern and eastern Europe. Throughout the campaign, the highest concentrations of PAHs, OPAHs and NPAHs were found in the sub-micrometre fraction of particulate matter (PM_1). Due to redistribution, the mass median diameter was shifted to higher values in long-range-transported aerosols.

Data availability. The data used in this study are archived and distributed through the KEEPER service of the Max Planck Digital Library (https://keeper.mpdl.mpg.de, last access: 12 December 2021, Max Planck Society, KEEPER, 2021) and have been available from August 2019 to all scientists agreeing to the AQABA protocol.

Supplement. The supplement related to this article is available online at: https://doi.org/10.5194/acp-22-8739-2022-supplement.

Author contributions. MW evaluated the data and wrote the manuscript. GL supervised this study. MI and RP did the sampling. MK, MI and EGS provided the data about alkylated PAHs and wrote this part. PPo performed the PMF and wrote the part. BN created the FLEXPART Lagrangian particle dispersion model results. JK provided the data about metals. PK and PPř performed the PAH, NPAH and OPAH sample preparation and analysis. IT created GPS plots and provided NO_x and O_3 data. NF, PE and JNC contributed measurements of NO_2, NO_x, NO_y, O_3 and SO_2. RR and ST provided OH radical data. BAMB and JW were involved in the discussion about the sources. The stack filter and other information about bypassing ships as well as BC and surface PAH concentrations was provided by FD and SC. HH took responsibility for the scientific coordination of the field campaign on board the research vessel. JL designed the AQABA campaign. GL designed this study, supported by EGS and UP. All authors contributed to data interpretation, discussion and manuscript revision.

Competing interests. At least one of the (co-)authors is a member of the editorial board of *Atmospheric Chemistry and Physics*. The peer-review process was guided by an independent editor, and the authors also have no other competing interests to declare.

Disclaimer. This publication reflects only the author's view, and the European Commission is not responsible for any use that may be made of the information it contains.

Publisher's note: Copernicus Publications remains neutral with regard to jurisdictional claims in published maps and institutional affiliations.

Acknowledgements. We thank Hays Ships Ltd, Captain Pavel Kirzner and the *Kommandor Iona's* ship crew for the great support. We would like to thank Marcel Dorf and Claus Koeppel for the organisation of the campaign, Hartwig Harder (MPIC) for the management on board, and all other participants and supporters of the campaign. We thank Benedikt Steil for processing meteorological data and Jan Schuladen (MPIC) for the data about the actinic flux. We also thank Abdulaziz al Senafi (Kuwait Inst. of Scientific Research). In addition, we thank Ondrej Sanka (MU) for the assistance with the plotting of sampling stretches.

Financial support. This research was supported by the Max Planck Society, the Czech Ministry of Education, Youth and Sports – Research Infrastructure RECETOX RI (no. LM2018121 and CZ.02.1.01/0.0/0.0/16_013/0001761), the project CETOCOEN EXCELLENCE (no. CZ.02.1.01/0.0/0.0/17_043/0009632) and the Czech Science Foundation (GACR 20-07117S). This project was supported by the European Union's Horizon 2020 Research and Innovation programme under grant agreement no. 857560.

The article processing charges for this open-access publication were covered by the Max Planck Society.

Review statement. This paper was edited by Sergey A. Nizkorodov and reviewed by two anonymous referees.

References

Abbas, I., Badran, G., Verdin, A., Ledoux, F., Roumie, M., and Courcot, D.: Polycyclic aromatic hydrocarbon derivatives in airborne particulate matter: sources, analysis and toxicity, Environ. Chem. Lett., 16, 439–475, https://doi.org/10.1016/j.envres.2016.01.041, 2018.

Albinet, A., Leoz-Garziandia, E., Budzinski, H., and Villenave, E.: Polycyclic aromatic hydrocarbons (PAHs), nitrated PAHs and oxygenated PAHs in ambient air of the Marseilles area (south

of France): concentrations and sources, Sci. Total Environ., 384, 280–292, https://doi.org/10.1016/j.scitotenv.2007.04.028, 2007.

Albinet, A., Leoz-Garziandia, E., Budzinski, H., Villenave, E., and Jaffrezo, J. L.: Nitrated and oxygenated derivatives of polycyclic aromatic hydrocarbons in the ambient air of two French alpine valleys, Part 1: concentrations, sources and gas/particle partitioning, Atmos. Environ., 42, 43–54, https://doi.org/10.1016/j.atmosenv.2007.10.009, 2008.

Alves, C. A., Vicente, A. M., Custódio, D., Cerqueira, M., Nunes, T., Pio, C., Lucarelli, F., Calzolai, G., Nava, S., Diapouli, E., Eleftheriadis, K., Querol, X., and Bandowe, B. A. M.: Polycyclic aromatic hydrocarbons and their derivatives (nitro-PAHs, oxygenated PAHs, and azaarenes) in $PM_{2.5}$ from southern European cities, Sci. Total Environ., 595, 494–504, https://doi.org/10.1016/j.scitotenv.2017.03.256, 2017.

Andersson, J. T. and Achten, C.: Time to say goodbye to the 16 EPA PAHs? Toward an up-to-date use of PACs for environmental purposes, Polycycl. Aromat. Comp., 35, 330–354, https://doi.org/10.1080/10406638.2014.991042, 2015.

Arey, J., Zielinska, B., Atkinson, R., Winer, A. M., Ramdahl, T., and Pitts, J. N.: The formation of nitro-PAH from gas-phase reactions of fluoranthene and pyrene with the OH radical in the presence of NO_x, Atmos. Environ., 20, 2339–2345, https://doi.org/10.1016/0004-6981(86)90064-8, 1986.

Atkinson, R. and Arey, J.: Atmospheric chemistry of gas-phase polycyclic aromatic hydrocarbons: formation of atmospheric mutagens, Environ. Health Persp., 102, 117–126, https://doi.org/10.1289/ehp.94102s4117, 1994.

Atkinson, R. and Arey, J.: Mechanisms of the gas-phase reactions of aromatic hydrocarbons and PAHs with OH and NO_3 radicals, Polycycl. Aromat. Compd., 27, 15–40, https://doi.org/10.1080/10406630601134243, 2007.

Atkinson, R., Aschmann, S. M., Arey, J., Zielinska, B., and Schuetzle, D.: Gas-phase atmospheric chemistry of 1-nitronaphthalene and 2-nitronaphthalene and 1,4-naphthoquinone, Atmos. Environ., 23, 2679–2690, https://doi.org/10.1016/0004-6981(89)90548-9, 1989.

Atkinson, R., Arey, J., Zielinska, B., and Aschmann, S. M.: Kinetics and nitro-products of the gas-phase OH and NO_3 radical-initiated reactions of naphthalene-d8, Fluoranthene-d10, and pyrene, Int. J. Chem. Kinet., 22, 999–1014, https://doi.org/10.1002/kin.550220910, 1990.

Bamford, H. A. and Baker, J. E.: Nitro-polycyclic aromatic hydrocarbon concentrations and sources in urban and suburban atmospheres of the mid-Atlantic region, Atmos. Environ., 37, 2077–2091, https://doi.org/10.1016/S1352-2310(03)00102-X, 2003.

Bamford, H. A., Bezabeh, D. Z., Schantz, M. M., Wise, S. A., and Baker, J. E.: Determination and comparison of nitrated-polycyclic aromatic hydrocarbons measured in air and diesel particulate reference materials, Chemosphere, 50, 575–587, https://doi.org/10.1016/S0045-6535(02)00667-7, 2003.

Bandowe, B. A. M. and Meusel, H.: Nitrated polycyclic aromatic hydrocarbons (nitro-PAHs) in the environment – A review, Sci. Total Environ., 581–582, 237–257, https://doi.org/10.1016/j.scitotenv.2016.12.115, 2017.

Bandowe, B. A. M., Meusel, H., Huang, R.-J., Ho, K., Cao, J., Hoffmann, T., and Wilcke, W.: $PM_{2.5}$-bound oxygenated PAHs, nitro-PAHs and parent-PAHs from the atmosphere of a Chinese megacity: seasonal variation, sources and cancer risk assessment, Sci. Total Environ., 473–474, 77–87, https://doi.org/10.1016/j.scitotenv.2013.11.108, 2014.

Baek, S. O., Field, R. A., Goldstone, M. E., Kirk, P. W., Lester, J. N., and Perry, R.: A review of atmospheric polycyclic aromatic hydrocarbons: Sources, fate and behaviour, Water Air Soil Pollut., 60, 279–300, https://doi.org/10.1007/BF00282628, 1991.

Bezabeh, D. Z., Bamford, H. A., Schantz, M. M., and Wise, S. A.: Determination of nitrated polycyclic aromatic hydrocarbons in diesel particulate-related standard reference materials by using gas chromatography/mass spectrometry with negative ion chemical ionization, Anal. Bioanal. Chem., 375, 381–388, https://doi.org/10.1007/s00216-002-1698-8, 2003.

Bläsing, M., Kistler, M., and Lehndorff, E.: Emission fingerprint of inland navigation vessels compared with road traffic, domestic heating and ocean-going vessels, Org. Geochem., 99, 1–9, https://doi.org/10.1016/j.orggeochem.2016.05.009, 2016.

Bolton, J. L., Trush, M. A., Penning, T. M., Dryhurst, G., and Monks, T. J.: Role of quinones in toxicology, Chem. Res. Toxicol., 13, 135–160, https://doi.org/10.1021/tx9902082, 2000.

Brorström-Lundén, E., Remberger, M., Kaj, L., Hansson, K., Palm Cousins, A., Andersson, H., Haglund, P., Ghebremeskel, M., and Schlabach, M.: Results from the Swedish national screening programme 2008: Screening of unintentionally produced organic contaminants, report B1944, Swedish Environmental Research Institute (IVL), Gothenburg, Sweden, 2010.

Bourtsoukidis, E., Ernle, L., Crowley, J. N., Lelieveld, J., Paris, J.-D., Pozzer, A., Walter, D., and Williams, J.: Non-methane hydrocarbon (C_2–C_8) sources and sinks around the Arabian Peninsula, Atmos. Chem. Phys., 19, 7209–7232, https://doi.org/10.5194/acp-19-7209-2019, 2019.

Bourtsoukidis, E., Pozzer, A., Sattler, T., Matthaios, V. N., Ernle, L., Edtbauer, A., Fischer, H., Könemann, T., Osipov, S., Paris, J.-D., Pfannerstill, E. Y., Stönner, C., Tadic, I., Walter, D., Wang, N., Lelieveld, J., and Williams, J.: The Red Sea Deep Water is a potent source of atmospheric ethane and propane, Nat. Commun., 11, 447, https://doi.org/10.1038/s41467-020-14375-0, 2020.

Budzinski, H., Garrigues, P., Connan, J., Devillers, J., Domine, D., Radke, M., and Oudins, J. L.: Alkylated phenanthrene distributions as maturity and origin indicators in crude oils and rock extracts, Geochim. Cosmochim. Ac., 59, 2043–2056, https://doi.org/10.1016/0016-7037(95)00125-5, 1995.

Castro-Jiménez, J., Berrojalbiz, N., Wollgast, J., and Dachs, J.: Polycyclic aromatic hydrocarbons (PAHs) in the Mediterranean Sea: Atmospheric occurrence, deposition and decoupling with settling fluxes in the water column, Environ. Pollut., 166, 40–47, https://doi.org/10.1016/j.envpol.2012.03.003, 2012.

Caumo, S., Vicente, A., Custodio, D., Alves, C., and Vasconcellos, P.: Organic compounds in particulate and gaseous phase collected in the neighbourhood of an industrial complex in Sao Paulo (Brazil), Air Qual. Atmos. Hlth., 11, 271–283, https://doi.org/10.1007/s11869-017-0531-7, 2018.

Celik, S., Drewnick, F., Fachinger, F., Brooks, J., Darbyshire, E., Coe, H., Paris, J.-D., Eger, P. G., Schuladen, J., Tadic, I., Friedrich, N., Dienhart, D., Hottmann, B., Fischer, H., Crowley, J. N., Harder, H., and Borrmann, S.: Influence of vessel characteristics and atmospheric processes on the gas and particle phase of ship emission plumes: in situ measurements in the Mediterranean Sea and around the Arabian Peninsula, At-

mos. Chem. Phys., 20, 4713–4734, https://doi.org/10.5194/acp-20-4713-2020, 2020.

Ciccioli, P., Cecinato, A., Brancaleoni, E., Frattoni, M., Zacchei, P., Miguel, A. H., and Vasconcellos, P. D.: Formation and transport of 2-nitrofluoranthene and 2-nitropyrene of photochemical origin in the troposphere, J. Geophys. Res.-Atmos., 101, 19567–19581, https://doi.org/10.1029/95JD02118, 1996.

Charrier, J. G. and Anastasio, C.: On dithiothreitol (DTT) as a measure of oxidative potential for ambient particles: evidence for the importance of soluble transition metals, Atmos. Chem. Phys., 12, 9321–9333, https://doi.org/10.5194/acp-12-9321-2012, 2012.

Clergé, A., Le Goff, J., Lopez, C., Ledauphin, J., and Delépée, R.: Oxy-PAHs: occurrence in the environment and potential genotoxic/mutagenic risk assessment for human health, Crit. Rev. Toxicol., 49, 302–328, https://doi.org/10.1080/10408444.2019.1605333, 2019.

Collins, J. F., Brown, J. P., Alexeeff, G. V., and Salmon, A. G.: Potency equivalency factors for some polycyclic aromatic hydrocarbons and polycyclic aromatic hydrocarbon derivatives, Regul. Toxicol. Pharm., 28, 45–54, https://doi.org/10.1006/rtph.1998.1235, 1998.

Dang, J., Shi, X., Zhang, Q., Hu, J., and Wang, W.: Mechanism and thermal rate constant for the gas-phase ozonolysis of acenaphthylene in the atmosphere, Sci. Total Environ., 514, 344–350, https://doi.org/10.1016/j.scitotenv.2014.12.009, 2015.

Degrendele, C., Okonski, K., Melymuk, L., Landlová, L., Kukučka, P., Čupr, P., and Klánová, J.: Size specific distribution of the atmospheric particulate PCDD/Fs, dl-PCBs and PAHs on a seasonal scale: Implications for cancer risks from inhalation, Atmos. Environ., 98, 410–416, https://doi.org/10.1016/j.atmosenv.2014.09.001, 2014.

Di Filippo, P., Riccardi, C., Pomata, D., and Buiarelli, F.: Concentrations of PAHs, and nitro- and methyl-derivatives associated with a size segregated urban aerosol, Atmos. Environ., 44, 2742–2749, https://doi.org/10.1016/j.atmosenv.2010.04.035, 2010.

Ding, X., Wang, X.-M., Xie, Z.-Q., Xiang, C.-H., Mai, B.-X., Sun, L.-G., Zheng, M., Sheng, G.-Y., Fu, J.-M., and Pöschl, U.: Atmospheric polycyclic aromatic hydrocarbons observed over the North Pacific Ocean and the Arctic area: spatial distribution and source identification, Atmos. Environ., 41, 2061–2072, https://doi.org/10.1016/j.atmosenv.2006.11.002, 2007.

Drotikova, T., Ali, A. M., Halse, A. K., Reinardy, H. C., and Kallenborn, R.: Polycyclic aromatic hydrocarbons (PAHs) and oxy- and nitro-PAHs in ambient air of the Arctic town Longyearbyen, Svalbard, Atmos. Chem. Phys., 20, 9997–10014, https://doi.org/10.5194/acp-20-9997-2020, 2020.

Drotikova, T., Dekhtyareva, A., Kallenborn, R., and Albinet, A.: Polycyclic aromatic hydrocarbons (PAHs) and their nitrated and oxygenated derivatives in the Arctic boundary layer: seasonal trends and local anthropogenic influence, Atmos. Chem. Phys., 21, 14351–14370, https://doi.org/10.5194/acp-21-14351-2021, 2021.

Durant, J. L., Busby Jr., W. F., Lafleur, A. L., Penman, B. W., and Crespi, C. L.: Human cell mutagenicity of oxygenated, nitrated and unsubstituted polycyclic aromatic hydrocarbons associated with urban aerosols, Mutat. Res., 371, 123–157, https://doi.org/10.1016/S0165-1218(96)90103-2, 1996.

ECHA (European Chemicals Agency): Grouping speeds up regulatory action – integrated regulatory strategy annual report 2020, European Chemicals Agency, https://doi.org/10.2823/092964, 2021.

Eger, P. G., Friedrich, N., Schuladen, J., Shenolikar, J., Fischer, H., Tadic, I., Harder, H., Martinez, M., Rohloff, R., Tauer, S., Drewnick, F., Fachinger, F., Brooks, J., Darbyshire, E., Sciare, J., Pikridas, M., Lelieveld, J., and Crowley, J. N.: Shipborne measurements of $ClNO_2$ in the Mediterranean Sea and around the Arabian Peninsula during summer, Atmos. Chem. Phys., 19, 12121–12140, https://doi.org/10.5194/acp-19-12121-2019, 2019.

El Alawi, Y. S., McConkey, B. J., Dixon, D. G., and Greenberg, B. M.: Measurement of short and long-term toxicity of polycyclic aromatic hydrocarbons using luminescent bacteria, Ecotox. Environ. Safe., 51, 12–21, https://doi.org/10.1006/eesa.2001.2108, 2002.

Fan, Z. H., Kamens, R. M., Hu, J. X., Zhang, J. B., and McDow, S.: Photostability of nitropolycyclic aromatic hydrocarbons on combustion soot particles in sunlight, Environ. Sci. Technol., 30, 1358–1364, https://doi.org/10.1016/1352-2310(94)00347-N, 1996.

Feilberg, A. and Nielsen, T.: Effect of aerosol chemical composition on the photodegradation of nitro-polycyclic aromatic hydrocarbons, Environ. Sci. Technol., 34, 789–797, https://doi.org/10.1021/es990566r, 2000.

Feilberg, A., Kamens, R. M., Strommen, M. R., and Nielsen, T.: Modeling the formation, decay, and partitioning of semivolatile nitro-polycyclic aromatic hydrocarbons (nitronaphthalenes) in the atmosphere, Atmos. Environ., 33, 1231–1243, https://doi.org/10.1016/S1352-2310(98)00275-1, 1999.

Feilberg, A., Poulsen, M. W. B., Nielsen, T., and Skov, H.: Occurrence and sources of particulate nitro-polycyclic aromatic hydrocarbons in ambient air in Denmark, Atmos. Environ., 35, 353–366, https://doi.org/10.1016/S1352-2310(00)00142-4, 2001.

Finlayson-Pitts, B. J. and Pitts Jr., J. N.: Chemistry of the upper and lower atmosphere, 1st Edn., Academic Press, New York, United States, 1999.

Friedrich, N., Eger, P., Shenolikar, J., Sobanski, N., Schuladen, J., Dienhart, D., Hottmann, B., Tadic, I., Fischer, H., Martinez, M., Rohloff, R., Tauer, S., Harder, H., Pfannerstill, E. Y., Wang, N., Williams, J., Brooks, J., Drewnick, F., Su, H., Li, G., Cheng, Y., Lelieveld, J., and Crowley, J. N.: Reactive nitrogen around the Arabian Peninsula and in the Mediterranean Sea during the 2017 AQABA ship campaign, Atmos. Chem. Phys., 21, 7473–7498, https://doi.org/10.5194/acp-21-7473-2021, 2021.

Gao, S., Zhang, Y., Meng, J., and Shu, J.: Online investigations on ozonation products of pyrene and benz[a]anthracene particles with a vacuum ultraviolet photoionization aerosol time-of-flight mass spectrometer, Atmos. Environ., 43, 3319–3325, https://doi.org/10.1016/j.atmosenv.2009.04.021, 2009.

Gao, Y., Lyu, Y., and Li, X.: Size distribution of airborne particle-bound PAHs and o-PAHs and their implications for dry deposition, Environ. Sci.-Proc. Imp., 21, 1184–1192, https://doi.org/10.1039/c9em00174c, 2019.

Garcia, K. O., Teixeira, E. C., Agudelo-Castañeda, D. M., Braga, M., Alabarse, P. G., Wiegand, F., Kautzmann, R. M., and Silva, L. F. O.: Assessment of nitro-polycyclic aromatic hydrocarbons in PM_1 near an area of heavy-duty traffic, Sci. Total Environ., 479–480, 57–65, https://doi.org/10.1016/j.scitotenv.2014.01.126, 2014.

Gogou, A., Stratigakis, N., Kanakidou, M., and Stephanou, E. G.: Organic aerosols in Eastern Mediterranean: components source reconciliation by using molecular markers and atmospheric back trajectories, Org. Geochem., 25, 79–96, https://doi.org/10.1016/S0146-6380(96)00105-2, 1996.

González-Gaya, B., Martínez-Varela, A., Vila-Costa, M., Casal, P., Cerro-Gálvez, E., Berrojalbiz, N., and Jiménez, B.: Biodegradation as an important sink of aromatic hydrocarbons in the oceans, Nat. Geosci., 12, 119–125, https://doi.org/10.1038/s41561-018-0285-3, 2019.

Harrison, R. M., Alam, M. S., Dang, J., Ismail, I. M., Basahi, J., Alghamdi, M. A., Hassan, I. A., and Khoder, M.: Relationship of polycyclic aromatic hydrocarbons with oxy(quinone) and nitro derivatives during air mass transport, Sci. Total Environ., 572, 1175–118, https://doi.org/10.1016/j.scitotenv.2016.08.030, 2016.

Helmig, D. and Harger, W. P.: OH radical-initiated gas-phase reaction-products of phenanthrene, Sci. Total Environ., 148, 11–21, https://doi.org/10.1016/0048-9697(94)90368-9, 1994.

Hens, K., Novelli, A., Martinez, M., Auld, J., Axinte, R., Bohn, B., Fischer, H., Keronen, P., Kubistin, D., Nölscher, A. C., Oswald, R., Paasonen, P., Petäjä, T., Regelin, E., Sander, R., Sinha, V., Sipilä, M., Taraborrelli, D., Tatum Ernest, C., Williams, J., Lelieveld, J., and Harder, H.: Observation and modelling of HO_x radicals in a boreal forest, Atmos. Chem. Phys., 14, 8723–8747, https://doi.org/10.5194/acp-14-8723-2014, 2014.

Hussain, M., Madl, P., and Khan, A.: Lung deposition predictions of airborne particles and the emergence of contemporary diseases, part-I, Health, 2, 51–59, 2011.

Iakovides, M., Stephanou, E. G., Apostolaki, M., Hadjicharalambous, M., Evans, J. S., Koutrakis, P., and Achilleos, S.: Study of the occurrence of airborne polycyclic aromatic hydrocarbons associated with respirable particles in two coastal cities at Eastern Mediterranean: Levels, source apportionment, and potential risk for human health, Atmos. Environ., 213, 170–184, https://doi.org/10.1016/j.atmosenv.2019.05.059 2019.

Iakovides, M., Apostolaki, M., and Stephanou, E. G.: PAHs, PCBs and organochlorine pesticides in the atmosphere of Eastern Mediterranean: Investigation of their occurrence, sources and gas-particle partitioning in relation to air mass transport pathways, Atmos. Environ., 244, 117931, https://doi.org/10.1016/j.atmosenv.2020.117931, 2021.

IARC (International Agency for Research on Cancer): Polynuclear aromatic compounds. Part 1. Chemical, environmental and experimental data. IARC monographs on the evaluation of carcinogenic risk of chemicals to humans, IARC, Vol. 32, Lyon, France, 978-92-832-1232-4, 1983.

IARC (International Agency for Research on Cancer): Some chemicals present in industrial and consumer products, food and drinking-water, IARC, Vol. 101, Lyon, France, 978-92-832-1324-6, 2012a.

IARC (International Agency for Research on Cancer): Diesel and gasoline exhausts and some nitroarenes, IARC monographs on the evaluation of carcinogenic risk of chemicals to humans, IARC, Vol. 105, Lyon, France, 2012b.

IARC (International Agency for Research on Cancer): Agents classified by the IARC monographs, Vol. 1–123, http://monographs.iarc.fr/ENG/Classification/ClassificationsAlphaOrder.pdf (last access: 4 January 2022), 2018.

Idowu, O., Semple, K. T., Ramadass, K., O'Connor, W., Hansbro, P., and Thavamani, P.: Beyond the obvious: Environmental health implications of polar polycyclic aromatic hydrocarbons, Environ. Int., 123, 543–557, https://doi.org/10.1016/j.envint.2018.12.051, 2019.

Jang, M. and McDow, S. R.: Products of benz[a]anthracene photodegradation in the presence of known organic constituents of atmospheric aerosols, Environ. Sci. Technol., 31, 1046–1053, https://doi.org/10.1021/es960559s, 1997.

Jariyasopit, N., Harner, T., Shin, C., and Park, R.: The effects of plume episodes on PAC profiles in the athabasca oil sands region, Environ. Pollut., 282, 1–9, https://doi.org/10.1016/j.envpol.2021.117014, 2021.

Jaward, F. M., Barber, J. L., Booij, K., and Jones, K. C.: Spatial distribution of atmospheric PAHs and PCNs along a north–south Atlantic transect, Environ. Pollut., 132, 173–181, https://doi.org/10.1016/j.envpol.2004.03.029, 2004.

Jin, R., Zheng, M., Lammel, G., Bandowe, B. A. M., and Liu, G.: Chlorinated and brominated polycyclic aromatic hydrocarbons: Sources, formation mechanisms, and occurrence in the environment, Prog. Energ. Combust., 76, 100803, https://doi.org/10.1016/j.pecs.2019.100803, 2020.

Johansson, L., Jalkanen, J.-P., and Kukkonen, J.: Global assessment of shipping emissions in 2015 on a high spatial and temporal resolution, Atmos. Environ., 167, 403–415, https://doi.org/10.1016/j.atmosenv.2017.08.042, 2017.

Kamens, R. M., Zhi-Hua, F., Yao, Y., Chen, D., Chen, S., and Vartianen, M.: A methodology for modeling the formation and decay of nitro-PAH in the atmosphere, Chemosphere, 28, 1623–1632, https://doi.org/10.1016/0045-6535(94)90421-9, 1994.

Kautzman, K. E., Surratt, J. D., Chan, M. N., Chan, A. W. H., S. P., Chhabra, P. S., Dalleska, N. F., Wennberg, P. O., Flagan, R. C., and Seinfeld, J. H.: Chemical composition of gas- and aerosol-phase products from the photooxidation of naphthalene, J. Phys. Chem. A, 114, 913–934, https://doi.org/10.1021/jp908530s, 2010.

Keith, L. H.: The source of U.S. EPA's sixteen PAH priority pollutants, Polycycl. Aromat. Comp., 35, 147–160, https://doi.org/10.1080/10406638.2014.892886, 2015.

Kelly, J. M., Ivatt, P. D., Evans, M. J., Kroll, J. H., Hrdina, A. I. H., Kohale, I. N., White, F. M., Engelward, B. P., and Selin, N. E.: Global cancer risk from unregulated polycyclic aromatic hydrocarbons, GeoHealth, 5, e2021GH000401, https://doi.org/10.1029/2021GH000401, 2021.

Keyte, I. J., Harrison, R. M., and Lammel, G.: Chemical reactivity and long-range transport potential of polycyclic aromatic hydrocarbons – a review, Chem. Soc. Rev., 42, 9333–9391, https://doi.org/10.1039/C3CS60147A, 2013.

Keyte, I. J., Albinet, A., and Harrison, R. M.: On-road traffic emissions of polycyclic aromatic hydrocarbons and their oxy- and nitro- derivative compounds measured in road tunnel environments, Sci. Total Environ., 566–567, 1131–1142, https://doi.org/10.1016/j.scitotenv.2016.05.152, 2016.

Kim, S. K. and Chae, D. H.: Seasonal variation in diffusive exchange of polycyclic aromatic hydrocarbons across the air-seawater interface in coastal urban area, Mar. Pollut. Bull., 109, 221–229, https://doi.org/10.1016/j.marpolbul.2016.05.078, 2016.

Kitanovski, Z., Shahpoury, P., Samara, C., Voliotis, A., and Lammel, G.: Composition and mass size distribution of nitrated and oxygenated aromatic compounds in ambient particulate matter from southern and central Europe – implications for the origin, Atmos. Chem. Phys., 20, 2471–2487, https://doi.org/10.5194/acp-20-2471-2020, 2020.

Lammel, G.: Polycyclic aromatic compounds in the atmosphere – a review identifying research needs, Polycycl. Aromat. Compd., 35, 316–329, https://doi.org/10.1080/10406638.2014.931870, 2015.

Lammel, G., Meixner, F. X., Vrana, B., Efstathiou, C. I., Kohoutek, J., Kukučka, P., Mulder, M. D., Přibylová, P., Prokeš, R., Rusina, T. P., Song, G.-Z., and Tsapakis, M.: Bidirectional air–sea exchange and accumulation of POPs (PAHs, PCBs, OCPs and PBDEs) in the nocturnal marine boundary layer, Atmos. Chem. Phys., 16, 6381–6393, https://doi.org/10.5194/acp-16-6381-2016, 2016.

Lammel, G., Mulder, M. D., Shahpoury, P., Kukučka, P., Lišková, H., Přibylová, P., Prokeš, R., and Wotawa, G.: Nitro-polycyclic aromatic hydrocarbons – gas–particle partitioning, mass size distribution, and formation along transport in marine and continental background air, Atmos. Chem. Phys., 17, 6257–6270, https://doi.org/10.5194/acp-17-6257-2017, 2017.

Lammel, G., Kitanovski, Z., Kukučka, P., Novák, J., Arangio, A. M., Codling, G. P., Filippi, A., Hovorka, J., Kuta, J., Leoni, C., Přibylová, P., Prokeš, R., Sáňka, O., Shahpoury, P., Tong, H. J., and Wietzoreck, M.: Oxygenated and nitrated polycyclic aromatic hydrocarbons in ambient air levels, phase partitioning, mass size distributions, and inhalation bioaccessibility, Environ. Sci. Technol., 54, 2615–2625, https://doi.org/10.1021/acs.est.9b06820, 2020.

Lee, S., Hong, S., Liu, X., Kim, C., Jung, D., Yim, U. H., Shim, W. J., Khim, J. S., Giesy, J. P., and Choi, K.: Endocrine disrupting potential of PAHs and their alkylated analogues associated with oil spills, Environ. Sci.-Proc. Imp., 19, 1117–1125, https://doi.org/10.1039/C7EM00125H, 2017.

Lelieveld, J., Berresheim, H., Borrmann, S., Crutzen, P. J., Dentener, F. J., Fischer, H., Feichter, J., Flatau, P. J., Heland, J., Holzinger, R., Korrmann, R., Lawrence, M. G., Levin, Z., Markowicz, K. M., Mihalopoulos, N., Minikin, A., Ramanathan, V., de Reus, M., Roelofs, G. J., Scheeren, H. A., Sciare, J., Schlager, H., Schultz, M., Siegmund, P., Steil, B., Stephanou, E. G., Stier, P., Traub, M., Warneke, C., Williams, J., and Ziereis, H.: Global air pollution crossroads over the Mediterranean, Science, 298, 794–799, https://doi.org/10.1126/science.1075457, 2002.

Lelieveld, J., Hoor, P., Jöckel, P., Pozzer, A., Hadjinicolaou, P., Cammas, J.-P., and Beirle, S.: Severe ozone air pollution in the Persian Gulf region, Atmos. Chem. Phys., 9, 1393–1406, https://doi.org/10.5194/acp-9-1393-2009, 2009.

Lelieveld, J., Evans, J. S., Fnais, M., Giannadaki, D., and Pozzer, A.: The contribution of outdoor air pollution sources to premature mortality on a global scale, Nature, 525, 367–371, https://doi.org/10.1038/nature15371, 2015.

Lelieveld, J., Klingmuller, K., Pozzer, A., Poschl, U., Fnais, M., Daiber, A., and Munzel, T.: Cardiovascular disease burden from ambient air pollution in Europe reassessed using novel hazard ratio functions, Eur. Heart J., 40, 1590–1596, https://doi.org/10.1093/eurheartj/ehz135, 2019.

Li, W., Wang, C., Shen, H., Su, S., Shen, G., Huang, Y., Zhang, Y., Chen, Y., Chen, H., Lin, N., Zhuo, S., Zhong, Q., Wang, X., Liu, J., Li, B., Liu, W., and Tao, S.: Concentrations and origins of nitro-polycyclic aromatic hydrocarbons and oxy-polycyclic aromatic hydrocarbons in ambient air in urban and rural areas in northern China, Environ. Pollut., 197, 156–164, https://doi.org/10.1016/j.envpol.2014.12.019, 2015.

Lin, Y., Ma, Y., Qiu, X., Li, R., Fang, Y., Wang, J., Zhu, Y., and Hu, D.: Sources, transformation, and health implications of PAHs and their nitrated, hydroxylated, and oxygenated derivatives in $PM_{2.5}$ in Beijing, J. Geophys. Res., 120, 7219–7228, https://doi.org/10.1002/2015JD023628, 2015.

Lohmann, R. and Lammel, G.: Adsorptive and absorptive contributions to the gas-particle partitioning of polycyclic aromatic hydrocarbons: state of knowledge and recommended parametrization for modelling, Environ. Sci. Technol., 38, 3793–3803, https://doi.org/10.1021/es035337q, 2004.

Lohmann, R., Klánová, J., Přibylová, P., Lisková, H., Yonis, S., and Bollinger, K.: PAHs on a west-to-east transect across the tropical Atlantic Ocean, Environ. Sci. Technol. 47, 2570–2578, https://doi.org/10.1021/es304764e, 2013.

Lyu, Y., Guo, H., Cheng, T., and Li, X.: Particle size distributions of oxidative potential of lung-deposited particles: Assessing contributions from quinones and water-soluble metals, Environ. Sci. Technol., 52, 6592–6600, https://doi.org/10.1021/acs.est.7b06686, 2018.

Mandalakis, M., Tsapakis, M., Tsoga, A., and Stephanou, E. G.: Gas-particle concentrations and distribution of aliphatic hydrocarbons, PAHs, PCBs and PCDD/Fs in the atmosphere of Athens (Greece), Atmos. Environ., 36, 4023–4035, https://doi.org/10.1016/S1352-2310(02)00362-X, 2002.

Marino, F., Cecinato, A., and Siskos, P. A.: Nitro-PAH in ambient particulate matter in the atmosphere of Athens, Chemosphere, 40, 533–537, https://doi.org/10.1016/S0045-6535(99)00308-2, 2000.

Martinez, M., Harder, H., Kubistin, D., Rudolf, M., Bozem, H., Eerdekens, G., Fischer, H., Klüpfel, T., Gurk, C., Königstedt, R., Parchatka, U., Schiller, C. L., Stickler, A., Williams, J., and Lelieveld, J.: Hydroxyl radicals in the tropical troposphere over the Suriname rainforest: airborne measurements, Atmos. Chem. Phys., 10, 3759–3773, https://doi.org/10.5194/acp-10-3759-2010, 2010.

Max Planck Society, KEEPER: Max Planck Digital Library, [data set], https://keeper.mpdl.mpg.de, last access: 12 December 2021.

Menichini, E. and Monfredini, F.: A field comparison of "total suspended particles" and "PM_{10}" air samplers in collecting polycyclic aromatic hydrocarbons, Int. J. Environ. An. Ch., 61, 299–307, https://doi.org/10.1080/03067319508027245, 1995.

Meusel, H., Kuhn, U., Reiffs, A., Mallik, C., Harder, H., Martinez, M., Schuladen, J., Bohn, B., Parchatka, U., Crowley, J. N., Fischer, H., Tomsche, L., Novelli, A., Hoffmann, T., Janssen, R. H. H., Hartogensis, O., Pikridas, M., Vrekoussis, M., Bourtsoukidis, E., Weber, B., Lelieveld, J., Williams, J., Pöschl, U., Cheng, Y., and Su, H.: Daytime formation of nitrous acid at a coastal remote site in Cyprus indicating a common ground source of atmospheric HONO and NO, Atmos. Chem. Phys., 16, 14475–14493, https://doi.org/10.5194/acp-16-14475-2016, 2016.

Minero, C., Maurino, V., Borghesi, D., Pelizzetti, E., and Vione, D.: An overview of possible processes able to

account for the occurrence of nitro-PAHs in the Antarctic particulate matter, Microchem. J., 96, 213–216, https://doi.org/10.1016/j.microc.2009.07.013, 2010.

Nalin, F., Golly, B., Besombes, J.-L., Pelletier, C., Aujay, R., Verlhac, S., Dermigny, A., Fievet, A., Karoski, N., Dubois, P., Collet, S., Favez, O., and Albinet, A.: Fast oxidation processes from 90 emission to ambient air introduction of aerosol emitted by residential log wood stoves, Atmos. Environ., 143, 15–26, doi:10.1016/j.atmosenv.2016.08.002, 2016.

Nassar, H. F., Tang, N., Kameda, T., Toriba, A., Khoder, M. I., and Hayakawa, K.: Atmospheric concentrations of polycyclic aromatic hydrocarbons and selected nitrated derivatives in Greater Cairo, Egypt, Atmos. Environ., 45, 7352–7359, https://doi.org/10.1016/j.atmosenv.2011.07.043, 2011.

Nežiková, B., Degrendele, C., Bandowe, B. A. M., Šmejkalová, A. H., Kukučka, P., Martiník, J., Mayer, L., Prokeš, R., Přibylová, P., Klánová, J., and Lammel, G.: Three years of atmospheric concentrations of nitrated and oxygenated polycyclic aromatic hydrocarbons and oxygen heterocycles at a central European background site, Chemosphere, 269, 128738, https://doi.org/10.1016/j.chemosphere.2020.128738, 2021.

Novelli, A., Hens, K., Tatum Ernest, C., Kubistin, D., Regelin, E., Elste, T., Plass-Dülmer, C., Martinez, M., Lelieveld, J., and Harder, H.: Characterisation of an inlet pre-injector laser-induced fluorescence instrument for the measurement of atmospheric hydroxyl radicals, Atmos. Meas. Tech., 7, 3413–3430, https://doi.org/10.5194/amt-7-3413-2014, 2014.

OEHHA (California Office of Environmental Health Hazard Assessment): Chemicals, https://oehha.ca.gov/chemicals/, last access: 2 December 2021.

Perraudin, E., Budzinski, H., and Villenave, E.: Identification and quantification of primary ozonation products of phenanthrene and anthracene adsorbed on silica particles, Atmos. Environ., 41, 6005–6017, https://doi.org/10.1016/j.atmosenv.2007.03.010, 2007.

Pfannerstill, E. Y., Wang, N., Edtbauer, A., Bourtsoukidis, E., Crowley, J. N., Dienhart, D., Eger, P. G., Ernle, L., Fischer, H., Hottmann, B., Paris, J.-D., Stönner, C., Tadic, I., Walter, D., Lelieveld, J., and Williams, J.: Shipborne measurements of total OH reactivity around the Arabian Peninsula and its role in ozone chemistry, Atmos. Chem. Phys., 19, 11501–11523, https://doi.org/10.5194/acp-19-11501-2019, 2019.

Pisso, I., Sollum, E., Grythe, H., Kristiansen, N. I., Cassiani, M., Eckhardt, S., Arnold, D., Morton, D., Thompson, R. L., Groot Zwaaftink, C. D., Evangeliou, N., Sodemann, H., Haimberger, L., Henne, S., Brunner, D., Burkhart, J. F., Fouilloux, A., Brioude, J., Philipp, A., Seibert, P., and Stohl, A.: The Lagrangian particle dispersion model FLEXPART version 10.4, Geosci. Model Dev., 12, 4955–4997, https://doi.org/10.5194/gmd-12-4955-2019, 2019.

Polissar, A. V., Hopke, P. K., Paatero, P., Malm, W. C., and Sisler, J. F.: Atmospheric aerosol over Alaska: 2. Elemental composition and sources, J. Geophys. Res., 103, 19045–19057, https://doi.org/10.1029/98JD01212, 1998.

Pryor, S. C., Gallagher, M.; Sievering, H., Larsen, S. E., Barthelmie, R. J., Birsan, F., Nemitz, E., Rinne, J., Kulmala, M., Grönholm, T., Taipale, R., and Vesala, T.: A review of measurement and modelling results of particle atmosphere–surface exchange, Tellus B, 60, 42–75, https://doi.org/10.1111/j.1600-0889.2007.00298.x, 2008.

Ravindra, K., Sokhi, R., and Van Grieken, R.: Atmospheric polycyclic aromatic hydrocarbons: source attribution, emission factors and regulation, Atmos. Environ., 42, 2895–2921, https://doi.org/10.1016/j.atmosenv.2007.12.010, 2008.

Reisen, F. and Arey, J.: Atmospheric reactions influence seasonal PAH and nitro-PAH concentrations in the Los Angeles basin, Environ. Sci. Technol., 39, 64–73, https://doi.org/10.1021/es035454l, 2005.

Ringuet, J., Albinet, A., Leoz-Garziandia, E., Budzinski, H., and Villenave, E.: Reactivity of polycyclic aromatic compounds (PAHs, NPAHs and OPAHs) adsorbed on natural aerosol particles exposed to atmospheric oxidants, Atmos. Environ., 61, 15–22, https://doi.org/10.1016/j.atmosenv.2012.07.025, 2012a.

Ringuet, J., Leoz-Garziandia, E., Budzinski, H., Villenave, E., and Albinet, A.: Particle size distribution of nitrated and oxygenated polycyclic aromatic hydrocarbons (NPAHs and OPAHs) on traffic and suburban sites of a European megacity: Paris (France), Atmos. Chem. Phys., 12, 8877–8887, https://doi.org/10.5194/acp-12-8877-2012, 2012b.

Schaub, D., Brunner, D., Boersma, K. F., Keller, J., Folini, D., Buchmann, B., Berresheim, H., and Staehelin, J.: SCIAMACHY tropospheric NO_2 over Switzerland: estimates of NO_x lifetimes and impact of the complex Alpine topography on the retrieval, Atmos. Chem. Phys., 7, 5971–5987, https://doi.org/10.5194/acp-7-5971-2007, 2007.

Scipioni, C., Villanueva, F., Pozo, K., and Mabilia, R.: Preliminary characterization of polycyclic aromatic hydrocarbons, nitrated polycyclic aromatic hydrocarbons and polychlorinated dibenzo-p-dioxins and furans in atmospheric PM_{10} of an urban and a remote area of Chile, Environ. Technol., 33, 809–820, https://doi.org/10.1080/09593330.2011.597433, 2012.

Seibert, P. and Frank, A.: Source-receptor matrix calculation with a Lagrangian particle dispersion model in backward mode, Atmos. Chem. Phys., 4, 51–63, https://doi.org/10.5194/acp-4-51-2004, 2004.

Seinfeld, J. H. and Pandis, S. N.: Atmospheric Chemistry and Physics: From Air Pollution to Climate Change, Wiley, New York, USA, LCCN 2015043236, ISBN 9781118947401, 2016.

Shah, V., Jacob, D. J., Li, K., Silvern, R. F., Zhai, S., Liu, M., Lin, J., and Zhang, Q.: Effect of changing NO_x lifetime on the seasonality and long-term trends of satellite-observed tropospheric NO_2 columns over China, Atmos. Chem. Phys., 20, 1483–1495, https://doi.org/10.5194/acp-20-1483-2020, 2020.

Shen, J., Zhang, S., Lian, J., Kong, L., and Chen, J.: Benz[a]anthracene heterogeneous photochemical reaction on the surface of TiO_2 particles, Acta Phys. Chim. Sin., 23, 1531–1536, https://doi.org/10.1016/S1872-1508(07)60078-3, 2007.

Shiraiwa, M., Garland, R. M., and Pöschl, U.: Kinetic double-layer model of aerosol surface chemistry and gas-particle interactions (K2-SURF): Degradation of polycyclic aromatic hydrocarbons exposed to O_3, NO_2, H_2O, OH and NO_3, Atmos. Chem. Phys., 9, 9571–9586, https://doi.org/10.5194/acp-9-9571-2009, 2009.

Shiraiwa, M., Ueda, K., Pozzer, A., Lammel, G., Kampf, C. J., Fushimi, A., Enami, S., Arangio, A. M., Fröhlich-Nowoisky, J., Fujitani, Y., Furuyama, A., Lakey, P. S. J., Lelieveld, J., Lucas, K., Morino, Y., Pöschl, U., Takahama, S., Takami, A., Tong, H., Weber, B., Yoshino, A., and Sato, K.: Aerosol health ef-

fects from molecular to global scales, Environ. Sci. Technol., 51, 1354513567, https://doi.org/10.1021/acs.est.7b04417, 2017.

Škrdlíková, L., Landlová, L., Klánová, J., and Lammel, G.: Wet deposition and scavenging efficiency of gaseous and particulate phase polycyclic aromatic compounds at a central European suburban site, Atmos. Environ., 45, 4305–4312, https://doi.org/10.1016/j.atmosenv.2011.04.072, 2011.

Srivastava, D., Tomaz, S., Favez, O., Lanzafame, G. M., Golly, B., Besombes, J.-L., Alleman, L. Y., Jaffrezo, J.-L., Jacob, V., Perraudin, E., Villenave, E., and Albinet, A.: Speciation of organic fraction does matter for source apportionment. Part 1: A one-year campaign in Grenoble (France), Sci. Total Environ., 624, 1598–1611, https://doi.org/10.1016/j.scitotenv.2017.12.135, 2018.

Srogi, K.: Monitoring of environmental exposure to polycyclic aromatic hydrocarbons: a review, Environ. Chem. Lett., 5, 169–195, https://doi.org/10.1007/s10311-007-0095-0, 2007.

Stohl, A., Forster, C., Frank, A., Seibert, P., and Wotawa, G.: Technical note: The Lagrangian particle dispersion model FLEXPART version 6.2, Atmos. Chem. Phys., 5, 2461–2474, https://doi.org/10.5194/acp-5-2461-2005, 2005.

Streibel, T., Schnelle-Kreis, J., Czech, H., Harndorf, H., Jakobi, G., Jokiniemi, J., Karg, E., Lintelmann, J., Matuschek, G., Michalke, B., Müller, L., Orasche, J., Passig, J.,Radischat, C., Rabe, R., Reda, A., Rüger, C., Schwemer, T., Sippula, O., Stengel, B., Sklorz, M., Torvela, T., Weggler, B., and Zimmermann, R.: Aerosol emissions of a ship diesel engine operated with diesel fuel or heavy fuel oil, Environ. Sci. Pollut. R., 24, 10976–10991, https://doi.org/10.1007/s11356-016-6724-z, 2017.

Sverdrup, L. E., Ekelund, F., Krogh, P. H., Nielsen, T., and Johnsen, K.: Soil microbial toxicity of eight polycyclic aromatic compounds: effects on nitrification, the genetic diversity of bacteria, and the total number of protozoans, Environ. Toxicol. Chem., 21, 1644–1650, https://doi.org/10.1002/etc.5620210815, 2002a.

Sverdrup, L. E., Krogh, P. H., Nielsen, T., and Stenersen, J.: Relative sensitivity of three terrestrial invertebrate tests to polycyclic aromatic compounds, Environ. Toxicol. Chem., 21, 1927–1933, https://doi.org/10.1002/etc.5620210921, 2002b.

Tadic, I., Crowley, J. N., Dienhart, D., Eger, P., Harder, H., Hottmann, B., Martinez, M., Parchatka, U., Paris, J.-D., Pozzer, A., Rohloff, R., Schuladen, J., Shenolikar, J., Tauer, S., Lelieveld, J., and Fischer, H.: Net ozone production and its relationship to nitrogen oxides and volatile organic compounds in the marine boundary layer around the Arabian Peninsula, Atmos. Chem. Phys., 20, 6769–6787, https://doi.org/10.5194/acp-20-6769-2020, 2020.

Tang, N., Sato, K., Tokuda, T., Tatematsu, M., Hama, H., Suematsu, C., Kameda, T., Toriba, A., and Hayakawa, K.: Factors affecting atmospheric 1-, 2-nitropyrenes and 2-nitrofluoranthene in winter at Noto Peninsula, a remote background site, Japan, Chemosphere, 107, 324–330, https://doi.org/10.1016/j.chemosphere.2013.12.077, 2014.

Tobiszewski, M. and Namieśnik, J.: PAH diagnostic ratios for the identification of pollution emission sources, Environ. Pollut., 162, 110–119, https://doi.org/10.1016/j.envpol.2011.10.025, 2012.

Tomaz, S., Shahpoury, P., Jaffrezo, J. L., Lammel, G., Perraudin, E., Villenave, E., and Albinet, A.: One-year study of polycyclic aromatic compounds at an urban site in Grenoble (France): seasonal variations, gas/particle partitioning and cancer risk estimation, Sci. Total Environ., 565, 1071–1083, https://doi.org/10.1016/j.scitotenv.2016.05.137, 2016.

Tomaz, S., Jaffrezo, J.-L., Favez, O., Perraudin, E., Villenave, E., and Albinet, A.: Sources and atmospheric chemistry of oxy- and nitro-PAHs in the ambient air of Grenoble (France), Atmos. Environ., 161, 144–154, https://doi.org/10.1016/j.atmosenv.2017.04.042, 2017.

Tsapakis, M. and Stephanou, E. G.: Occurrence of gaseous and particulate polycyclic aromatic hydrocarbons in the urban atmosphere: study of sources and ambient temperature effect on the gas/particle concentration and distribution, Environ. Pollut., 133, 147–156, https://doi.org/10.1016/j.envpol.2004.05.012, 2005.

Tsapakis, M. and Stephanou, E. G.: Diurnal cycle of PAHs, nitro-PAHs, and oxy-PAHs in a high oxidation capacity marine background atmosphere, Environ. Sci. Technol., 41, 8011–8017, https://doi.org/10.1021/es071160e, 2007.

Turcotte, D., Akhtar, P., Bowerman, M., Kiparissis, Y., Brown, R. S., and Hodson, P. V.: Measuring the toxicity of alkylphenanthrenes to early life stages of medaka (Oryzias latipes) using partition controlled delivery, Environ. Toxicol. Chem., 30, 487–495, https://doi.org/10.1002/etc.404, 2011.

US EPA (United States Environmental Protection Agency): Estimation Programs Interface Suite™ for Microsoft® Windows, v 4.11, https://www.epa.gov/tsca-screening-tools/epi-suitetm-estimation-program-interface (last access: 5 January 2022) 2019.

Valavanidis, A., Vlachogianni, T., Triantafyllaki, S., Dassenakis, M., Androutsos, F., and Scoullos, M.: Polycyclic aromatic hydrocarbons in surface seawater and in indigenous mussels (Mytilus galloprovincialis) from coastal areas of the Saronikos Gulf (Greece), Estuar. Coast. Shelf S., 79, 733–739, https://doi.org/10.1016/j.ecss.2008.06.018, 2008.

van Drooge, B. L., Fernández, P., Grimalt, J. O., Stuchlík, E., Torres García, C. J., and Cuevas, E.: Atmospheric polycyclic aromatic hydrocarbons in remote European and Atlantic sites located above the boundary mixing layer, Environ. Sci. Pollut. R., 17, 1207–1216, https://doi.org/10.1007/s11356-010-0296-0, 2010.

Verma, V., Wang, Y., El-Afifi, R., Fang, T., Rowland, J., Russell, A. G., and Weber, R. J.: Fractionating ambient humic-like substances (HULIS) for their reactive oxygen species activity – Assessing the importance of quinones and atmospheric aging, Atmos. Environ., 120, 351–359, https://doi.org/10.1016/j.atmosenv.2015.09.010, 2015.

Vincenti, M., Maurino, V., Minero, C., and Pelizzetti, E.: Detection of nitro-substituted polycyclic aromatic hydrocarbons in the Antarctic airborne particulate, Int. J. Environ. An. Ch., 79, 257–272, https://doi.org/10.1080/03067310108044388, 2001.

Walgraeve, C., Demeestere, K., Dewulf, J., Zimmermann, R., and Van Langenhove, H.: Oxygenated polycyclic aromatic hydrocarbons in atmospheric particulate matter: molecular characterization and occurrence, Atmos. Environ., 44, 1831–1846, https://doi.org/10.1016/j.atmosenv.2009.12.004, 2010.

Wang, L., Atkinson, R., and Arey, J.: Formation of 9,10-phenanthrenequinone by atmospheric gas-phase reactions of phenanthrene, Atmos. Environ., 41, 2025–35, https://doi.org/10.1016/j.atmosenv.2006.11.008, 2007.

Wang, N., Edtbauer, A., Stönner, C., Pozzer, A., Bourtsoukidis, E., Ernle, L., Dienhart, D., Hottmann, B., Fischer, H., Schuladen, J., Crowley, J. N., Paris, J.-D., Lelieveld, J., and Williams, J.: Measurements of carbonyl compounds around the Arabian Peninsula: overview and model comparison, Atmos. Chem. Phys., 20, 10807–10829, https://doi.org/10.5194/acp-20-10807-2020, 2020.

Wassenaar, P. N. H. and Verbruggen, E. M. J.: Persistence, bioaccumulation and toxicity-assessment of petroleum UVCBs: A case study on alkylated three-ring PAHs, Chemosphere, 276, 130113, https://doi.org/10.1016/j.chemosphere.2021.130113, 2021.

Wei, C., Han, Y. M., Bandowe, B. A. M., Cao, J. J., Huang, R. J., Ni, H. Y., Tian, J., and Wilcke, W.: Occurrence, gas/particle partitioning and carcinogenic risk of polycyclic aromatic hydrocarbons and their oxygen and nitrogen containing derivatives in Xi'an, central China, Sci. Total Environ., 505, 814–822, https://doi.org/10.1016/j.scitotenv.2014.10.054, 2015.

WHO: Selected nitro-and nitro-oxy-polycyclic aromatic hydrocarbons, EHC (Environmental Health Criteria) 229, WHO Library, World Health Organization, ISBN 9241572299, 2003.

Wilson, J., Octaviani, M., Bandowe, B. A. M., Wietzoreck, M., Zetzsch, C., Pöschl, U., Berkemeier, T., and Lammel, G.: Modeling the formation, degradation, and spatiotemporal distribution of 2-nitrofluoranthene in the global atmosphere, Environ. Sci. Technol., 54, 14224–14234, https://doi.org/10.1021/acs.est.0c04319, 2020.

Xiong, Q., Yu, H., Wang, R., Wei, J., and Verma, V.: Rethinking dithiothreitol-based particulate matter oxidative potential: measuring dithiothreitol consumption versus reactive oxygen species generation, Environ. Sci. Technol., 51, 6507–6514, https://doi.org/10.1021/acs.est.7b01272, 2017.

Yunker, M. B., Macdonald, R. W., Vingarzan, R., Mitchell, R. H., Goyette, D., and Sylvestre, S.: PAHs in the Fraser river basin: a critical appraisal of PAH ratios as indicators of PAH source and composition, Org. Geochem., 33, 489–515, https://doi.org/10.1016/S0146-6380(02)00002-5, 2002.

Zhang, J., Yang, L., Mellouki, A., Chen, J., Chen, X., Gao, Y., Jiang, P., Li, Y., Yu, H., and Wang, W: Atmospheric PAHs, NPAHs, and OPAHs at an urban, mountainous, and marine sites in Northern China: Molecular composition, sources, and ageing, Atmos. Environ., 173, 256–264, https://doi.org/10.1016/j.atmosenv.2017.11.002, 2018.

Zhao, J., Zhang, Y., Wang, T., Sun, L., Yang, Z., Lin, Y., Chen, Y., and Mao, H.: Characterization of $PM_{2.5}$-bound polycyclic aromatic hydrocarbons and their derivatives (nitro-and oxy-PAHs) emissions from two ship engines under different operating conditions, Chemosphere, 225, 43–52, https://doi.org/10.1016/j.chemosphere.2019.03.022, 2019.

Zhao, J., Zhang, Y., Chang, J., Peng, S., Hong, N., Hu, J., Ly, J., Wang, T., and Mao, H.: Emission characteristics and temporal variation of PAHs and their derivatives from an ocean-going cargo vessel, Chemosphere, 249, 126194, https://doi.org/10.1016/j.chemosphere.2020.126194, 2020.

Zhao, Y., Cao, L., Zhou, Q., Que, Q., and Hong, B.: Effects of oil pipeline explosion on ambient particulate matter and their associated polycyclic aromatic hydrocarbons, Environ. Pollut., 196, 440–449, https://doi.org/10.1016/j.envpol.2014.11.012, 2015.

Zhuo, S., Du, W., Shen, G., Li, B., Liu, J., Cheng, H., Xing, B., and Tao, S.: Estimating relative contributions of primary and secondary sources of ambient nitrated and oxygenated polycyclic aromatic hydrocarbons, Atmos. Environ., 159, 126–134, https://doi.org/10.1016/j.atmosenv.2017.04.003, 2017.

Zielinska, B., Sagebiel, J., McDonald, J. D., Whitney, K., and Lawson, D. R.: Emission rates and comparative chemical composition from selected in-use diesel and gasoline-fueled vehicles, J. Air Waste Manage., 54, 1138–1150, https://doi.org/10.1080/10473289.2004.10470973, 2004.

Zimmermann, K., Atkinson, R., Arey, J., Kojima, Y., and Inazu, K.: Isomer distributions of molecular weight 247 and 273 nitro-PAHs in ambient samples, NIST Diesel SRM, and from radical-initiated chamber reactions, Atmos. Environ., 55, 431–439, https://doi.org/10.1016/j.atmosenv.2012.03.016, 2012.